

**Manuscript version: Author's Accepted Manuscript**

The version presented in WRAP is the author's accepted manuscript and may differ from the published version or Version of Record.

**Persistent WRAP URL:**

<http://wrap.warwick.ac.uk/136008>

**How to cite:**

Please refer to published version for the most recent bibliographic citation information. If a published version is known of, the repository item page linked to above, will contain details on accessing it.

**Copyright and reuse:**

The Warwick Research Archive Portal (WRAP) makes this work by researchers of the University of Warwick available open access under the following conditions.

© 2020 Elsevier. Licensed under the Creative Commons Attribution-NonCommercial-NoDerivatives 4.0 International <http://creativecommons.org/licenses/by-nc-nd/4.0/>.



**Publisher's statement:**

Please refer to the repository item page, publisher's statement section, for further information.

For more information, please contact the WRAP Team at: [wrap@warwick.ac.uk](mailto:wrap@warwick.ac.uk).

# Compressive resistance of high-strength and normal-strength steel circular hollow section members at elevated temperatures

Merih Kucukler

*School of Engineering, University of Warwick, Coventry, CV4 7AL, UK*

---

## Abstract

The compressive behaviour of hot-finished circular hollow section steel members in fire is investigated in this paper through numerical modelling. CHS members with high-strength steel grades of S690 and S460 are taken into consideration in addition to those made up of normal-strength grades S355, S275 and S235. Numerical models of circular hollow section (CHS) structural steel members able to replicate their response in fire are validated. Using the validated finite element models, extensive parametric studies are carried out for the purpose of exploring a broad range of factors influencing the cross-section and member buckling response of CHS steel members under axial compression at elevated temperatures. The accuracy and safety of the design recommendations provided in the European structural steel fire design standard EN 1993-1-2 for the determination of the axial compression resistances of CHS steel members in fire are assessed. New design methods able to provide accurate and safe estimations of the cross-section axial compression resistances and flexural buckling resistances of CHS steel members at elevated temperatures are proposed. The higher accuracy, reliability and safety of the proposed design methods relative to the existing design provisions in EN 1993-1-2 are illustrated.

*Keywords:* Circular hollow section (CHS); Finite element modelling; Geometrical Imperfections; High-strength steel; Instability in fire; Local buckling; S690 steel; S460 steel

---

## 1. Introduction

High-strength steel, defined as structural steel whose yield strength is greater 460 MPa according to EN 1993-1-12 [1] and 450 MPa according to AS 4100 [2], brings about significant advantages as a structural material, leading to decreased material consumptions and reduced self-weights for structural steel elements which result in more sustainable construction, decreased transportation and construction costs and easier and faster erection of structural steel members. In view of its advantages over mild steel, a significant research effort [3–13] has recently been focused the behaviour and design of high-strength steel structural elements, which may display structural response that is considerably different than

---

*Email address:* merih.kucukler@warwick.ac.uk (Merih Kucukler)

that of structural steel members made of normal-strength steel owing to the differences in the material behaviour. However, thus far, research studies on high-strength steel structural members have predominantly investigated their room temperature behaviour and design. The elevated temperature response and design of high-strength steel structural elements have received a relatively lower level of research interest [14–17].

Circular hollow section (CHS) steel members are widely used in structures owing to their aesthetic appearance, efficiency in resisting buckling in multiple directions and high torsional stiffness which effectively suppresses flexural-torsional instabilities. Combining the structural advantages offered by CHS members and the benefits of high-strength steel as construction material, steel manufacturers [18, 19] provide hot-finished CHS members up to 890 MPa in Europe, produced conforming to the fabrication requirements and tolerances set out in EN 10210 [20]. In many instances, high-strength steel CHS members and in some instances normal-strength CHS elements have slender cross-sections which make them susceptible to local buckling effects, resulting in significant reductions in their cross-section resistances. The room temperature cross-section behaviour and design of CHS steel members have been comprehensively investigated in the literature. However, their cross-section behaviour and design at elevated temperatures have been relatively unexplored. Unique design guidance for the cross-section strength estimations of CHS members in fire is also not provided in the European structural steel fire design guidance EN 1993-1-2 [21], which merely directs the designers to the relevant design provisions of the European room temperature structural steel design codes EN 1993-1-1 [22] and EN 1993-1-6 [23], despite the considerably different cross-section response of CHS elements in fire in comparison to their room temperature cross-section behaviour. In parallel to the lack of extensive research on the cross-section response of CHS structural members in fire, the flexural buckling behaviour of high-strength steel CHS columns at elevated temperatures has also not been thoroughly investigated in the literature. The existing column buckling design rules of EN 1993-1-2 [21] are based upon numerical simulations [24, 25] and physical experiments [26] that have been primarily focused on normal-strength steel I-section members. As part of the FIDESC4 [27] project supported by the European Commission Research Fund for Coal and Steel (RFCS), [28–36] have comprehensively investigated the behaviour of structural steel members with Class 4 sections in fire, which resulted in major developments in understanding the response of structural steel elements at elevated temperatures and the revisions of a number of design provisions of EN 1993-1-2 [21] which will be implemented in the upcoming version of the standard. However, in this project [27], the behaviour and design of only normal-strength I- and H-section steel members were investigated, signifying that further studies focusing on the structural response and design of high-strength steel elements in fire are necessary.

With the aim of addressing the existing gap of knowledge on the behaviour of CHS members at elevated temperatures, a research study focusing on the cross-section and flexural buckling behaviour of high-strength and normal-strength steel CHS members under axial compression in fire is carried out in this paper. Finite element models able to replicate the structural response of CHS steel members in fire are created and validated against experimental results in the literature. Using the validated finite element models, extensive numerical parametric studies are carried out on both the cross-section response and flexural

buckling behaviour of CHS steel members subjected to axial compression in fire, considering grade S690, S460, S355, S275 and S235 steels, different elevated temperature levels and various cross-section and global member slendernesses. The accuracy and safety of the existing design rules in EN 1993-1-2 [21] for the determination of the axial compression resistances of CHS members in fire are assessed against benchmark results obtained from the Geometrically and Materially Nonlinear Analyses with Imperfections (GMNIA) of the created finite element models. New design proposals leading to accurate and safe estimations of the ultimate cross-section axial compression resistances and flexural buckling resistances of CHS members in fire are put forward. The higher accuracy and safety of the new proposals relative to the existing design rules in EN 1993-1-2 [21] are illustrated. Note that in this paper, steels with yield strengths greater than 450 MPa are classified as high-strength steels. Moreover, it should also be emphasised that the design methods proposed in this paper is only applicable to CHS members; the proposed design methods will be extended to tubular steel members with other cross-section shapes such as square, rectangular and elliptical cross-sections in a future study.

## 2. Finite element modelling

In this section, the finite element models able to mimic the behaviour of CHS steel members at elevated temperatures are developed and validated against experimental studies from the literature. In the following sections, the validated finite element models will be utilised in the assessment of the accuracy of the existing provisions of EN 1993-1-2 [21] for the prediction of the structural response of CHS steel members under compression in fire and in the development of new design proposals leading to a more accurate assessment of their behaviour.

### 2.1. Element type and modelling assumptions

The finite element models were created using the finite element analysis software Abaqus in this paper [37]. Denoted as S4R in the Abaqus element library, a four-noded, reduced integration shell element able to account for transverse shear deformations and membrane stresses was utilised to create the finite element models in this study. This element type has previously been used to replicate the structural response of steel elements in similar applications [38–42]. In the finite element models, two planes of symmetry at mid-span and for half of the cross-section were exploited to improve the computational efficiency by using the quarter models of CHS members as shown in Fig. 1, adopting appropriate boundary conditions at the mid-length section and along the two longitudinal edges of the models in line with the approach followed in [43]. The appropriateness of the computationally efficient quarter model was verified against the results obtained from the full models of CHS stub columns and long columns. Note that for long CHS columns, the symmetry about the plane perpendicular to the global flexural buckling axis was exploited. A fine mesh with element size of  $0.1\sqrt{D/t}$ , where  $D$  is the outer diameter and  $t$  is the thickness, was adopted in the finite element models, which has been shown to provide accurate estimations of the local buckling response of CHS members in [44]. While this fine mesh was applied to all the

regions of the finite element models of CHS stub columns, it was applied only to the mid-span region of long CHS columns where local buckling is expected as shown in Fig. 1 (b); for the remainder regions of the finite element models of long CHS columns, a mesh size of  $0.4\sqrt{D}/t$  was adopted similar to the approach followed in [44]. Note that the length of the mid-span region where the increased mesh density was used was taken as four times of the local buckling wavelength of a CHS member. The finite element models were analysed isothermally where initially a uniform temperature increase to a predefined temperature value  $\theta$  was assumed, which was represented by the modification of the material response, and then the loading was applied at the designated elevated temperature value  $\theta$ . The modified Riks analysis [45, 46] was utilised to trace the full load-displacement response of CHS members.

## 2.2. Material modelling

To replicate the behaviour of CHS members made of normal-strength grade S355, S275 and S235 steels in fire, the four-stage elevated temperature material model provided in EN 1993-1-2 [21] for carbon steel was adopted, defining the elevated temperature stress versus strain relationship using the following equations:

$$\begin{aligned} \sigma &= \epsilon E_\theta \quad \text{for } \epsilon \leq \epsilon_{p,\theta}, \\ \sigma &= f_{p,\theta} - c + (b/a)\sqrt{a^2 - (\epsilon_{y,\theta} - \epsilon)^2} \quad \text{for } \epsilon_{p,\theta} \leq \epsilon \leq \epsilon_{y,\theta}, \\ \sigma &= f_{y,\theta} \quad \text{for } \epsilon_{y,\theta} \leq \epsilon \leq \epsilon_{t,\theta}, \\ \sigma &= f_{y,\theta} [1 - (\epsilon - \epsilon_{t,\theta}) / (\epsilon_{u,\theta} - \epsilon_{t,\theta})] \quad \text{for } \epsilon_{t,\theta} \leq \epsilon \leq \epsilon_{u,\theta}, \end{aligned} \quad (1)$$

where  $\sigma$  and  $\epsilon$  are the engineering stress and strain and  $E_\theta$ ,  $f_{p,\theta}$  and  $f_{y,\theta}$  are the Young's modulus, the proportional limit and the effective yield strength at temperature  $\theta$ , respectively. In eq. (1),  $\epsilon_{p,\theta}$  is the strain at proportional limit calculated as  $\epsilon_{p,\theta} = f_{p,\theta}/E_\theta$ ,  $\epsilon_{y,\theta}$  is the yield strain equal to 0.02 (i.e.  $\epsilon_{y,\theta} = 0.02$ ),  $\epsilon_{t,\theta}$  is the limiting strain for yield strength taken as 0.15 (i.e.  $\epsilon_{t,\theta} = 0.15$ ) and  $\epsilon_{u,\theta}$  is the ultimate strain equal to 0.20 (i.e.  $\epsilon_{u,\theta} = 0.20$ ). The auxiliary coefficients  $a$ ,  $b$  and  $c$  used in eq. (1) are determined as given below:

$$\begin{aligned} a &= \sqrt{(\epsilon_{y,\theta} - \epsilon_{p,\theta})(\epsilon_{y,\theta} - \epsilon_{p,\theta} + c/E_\theta)}, \\ b &= \sqrt{c(\epsilon_{y,\theta} - \epsilon_{p,\theta})E_\theta + c^2}, \\ c &= \frac{(f_{y,\theta} - f_{p,\theta})^2}{(\epsilon_{y,\theta} - \epsilon_{p,\theta})E_\theta - 2(f_{y,\theta} - f_{p,\theta})}. \end{aligned} \quad (2)$$

As shown in Fig. 2 (a), the elevated temperature effective yield strength  $f_{y,\theta}$  and proportional limit  $f_{p,\theta}$  are calculated by multiplying the elevated temperature yield strength reduction factor  $k_{y,\theta}$  and proportional limit reduction factor  $k_{p,\theta}$  by the room temperature yield strength  $f_y$  (i.e.  $f_{y,\theta} = k_{y,\theta}f_y$  and  $f_{p,\theta} = k_{p,\theta}f_y$ ), whereas the elevated temperature Young's modulus  $E_\theta$  is calculated by multiplying the elevated temperature Young's modulus reduction factor  $k_{E,\theta}$  by the room temperature Young's modulus of carbon steel  $E$  (i.e.  $E_\theta = k_{E,\theta}E$ ). In this

paper, the values of  $k_{y,\theta}$ ,  $k_{p,\theta}$  and  $k_{E,\theta}$  provided in EN 1993-1-2 [21] and illustrated in Fig. 2 (b) were used for grade S355, S275 and S235 steels, where  $k_{p0.2,\theta}$  is the elevated temperature 0.2% proof strength reduction factor multiplied by the yield strength  $f_y$  to determine the elevated temperature 0.2% proof strength  $f_{p0.2,\theta}$  (i.e.  $f_{p0.2,\theta} = k_{p0.2,\theta} f_y$ ). Note that the engineering stress-strain relationship given by eq. (2) was transformed into a true stress-strain relationship for input into the finite element models.

While the EN 1993-1-2 [21] elevated temperature material model given by eq. (2), which was originally derived in [47] using results from a series of anisothermal tests on steel beams, leads to accurate estimations of the elevated temperature stress-strain response of normal-strength steels, it has been shown in the literature that it overestimates the elevated temperature stress-strain response of high strength steels [48–50]. Thus, the use of the EN 1993-1-2 [21] four stage material model to define the stress-strain behaviour of high-strength steels may lead to overestimations of the ultimate strengths of high-strength steel elements in fire. Considering this, the EN 1993-1-2 [21] material stress-strain model was adopted only in the finite element models of CHS columns made of grade S355, S275 and S235 steels in this paper. For the case of S690 and S460 grade steels, the two-stage elevated temperature material model put forward by Fang and Chan [17, 51] for high strength grade S690 and S460 steels, based on the elevated temperature material model for high-strength steels recommended by Chen and Young [14], was adopted in this study, which is defined using the equations below:

$$\begin{aligned} \epsilon &= \frac{\sigma}{E_\theta} + 0.002 \left( \frac{\sigma}{f_{p0.2,\theta}} \right)^{n_\theta} & \text{for } \sigma \leq f_{p0.2,\theta}, \\ \epsilon &= \frac{\sigma - f_{p0.2,\theta}}{E_{p0.2,\theta}} + \epsilon_{u,\theta} \left( \frac{\sigma - f_{p0.2,\theta}}{f_{u,\theta} - f_{p0.2,\theta}} \right)^{m_\theta} + \epsilon_{p0.2,\theta} & \text{for } f_{p0.2,\theta} \leq \sigma \leq f_{u,\theta}, \end{aligned} \quad (3)$$

where  $\epsilon_{p0.2,\theta}$  is the total strain corresponding to  $f_{p0.2,\theta}$ ,  $n_\theta$  and  $m_\theta$  are the exponents defining the nonlinearity of the stress-strain curve and  $E_{p0.2,\theta}$  is the tangent modulus at  $f_{p0.2,\theta}$ , which is calculated by

$$E_{p0.2,\theta} = \frac{E_\theta}{(1 + 0.002n_\theta E_\theta / f_{p0.2,\theta})}. \quad (4)$$

The exponents  $n_\theta$  and  $m_\theta$  can be determined using the following expressions for grade S690 steel [51]:

$$\begin{aligned} n_\theta &= 7 - \frac{\theta}{250}, \\ m_\theta &= 1.6 + \frac{\theta}{600}, \end{aligned} \quad (5)$$

and the following equations for grade S460 steel [17, 51]:

$$\begin{aligned} n_\theta &= 12 - \frac{\theta}{100}, \\ m_\theta &= 2.1 + \frac{3\theta}{600}. \end{aligned} \quad (6)$$

Note that the elevated temperature material model given by eq. (3) was derived in [14, 17, 51] considering the two-stage compound Ramberg-Osgood material model put forward by Mirambell and Real [52] to represent the stress-strain response of stainless steels at room temperature and has been shown to provide accurate estimations of the elevated temperature stress-strain response of high-strength steels [14, 17, 51].

In this paper, the elevated temperature material properties (i.e.  $E_\theta$ ,  $f_{p0.2,\theta}$ ,  $f_{y,\theta}$ ,  $f_{u,\theta}$  and  $\epsilon_{u,\theta}$ ) of grade S690 and S460 steels were determined using the results from the elevated temperature material tests carried out on high-strength grade S690 and S460 steels by Qiang et al. [53] and Qiang et al. [54], respectively. The room temperature yield strength  $f_y$ , ultimate tensile strength  $f_u$  and strain  $\epsilon_u$  and the Young's modulus  $E$  for grade S690 and S460 steel obtained from the room temperature material tests in [53, 54] were multiplied by the material reduction factors (i.e.  $k_{E,\theta}$ ,  $k_{p0.2,\theta}$ ,  $k_{y,\theta}$  and  $k_{u,\theta}$ ) derived in [53, 54] to determine their values at particular elevated temperature levels  $\theta$  in this paper, i.e.  $E_\theta = k_{E,\theta}E$ ,  $f_{p0.2,\theta} = k_{p0.2,\theta}f_y$ ,  $f_{y,\theta} = k_{y,\theta}f_y$ ,  $f_{u,\theta} = k_{u,\theta}f_y$  and  $\epsilon_{u,\theta} = k_{\epsilon_u,\theta}\epsilon_u$ . The room temperature material properties of grade S690 steel were thus taken as  $E = 204690$  MPa,  $f_y=789$  MPa,  $\sigma_u=821$  MPa and  $\epsilon_u=0.051$  as obtained in [53] and those of grade S460 steel were taken as  $E = 202812$  MPa,  $f_y=504$  MPa,  $\sigma_u=640$  MPa and  $\epsilon_u=0.115$  as determined in [54]. The corresponding material reduction factors for S690 and S460 steels provided in [53, 54] and adopted in this study are shown in Table 1 and Table 2 in addition to the Ramberg-Osgood parameters  $n_\theta$  and  $m_\theta$  calculated using eq. (5) and eq. (6) for different elevated temperature levels. Fig. 3 shows a comparison of the Young's modulus  $k_{E,\theta}$  and yield strength reduction factors  $k_{y,\theta}$  adopted for high-strength grade S690 and S460 steels against those adopted for normal-strength grade S355, S275 and S235 steels. It can be seen from the figure that the yield strength reduction factors  $k_{y,\theta}$  for grade S690 and S460 steels are lower than those for normal-strength steels, while the Young's modulus reduction is less severe for grade S690 steel but more pronounced for grade S460 steel relative to the Young's modulus reduction rates of normal-strength grade S355, S275 and S235 steels. The elevated temperature stress-strain response of grade S690 and S460 steels determined using eq. (3) and the elevated temperature material properties from [53, 54] are compared against the elevated temperature stress-strain curves obtained from the material tests by [53, 54] in Fig. 4, showing that the agreement between the elevated temperature stress-strain curves used in the finite element models and those obtained from the material tests is good.

### 2.3. Boundary conditions

The boundary conditions adopted in the finite element models of CHS stub columns and long columns are illustrated in Fig. 1. As can be seen from the figure, the end displacements and rotations were linked to a reference point located at the centroid of the cross-section through a rigid body kinematic coupling, where the boundary conditions and axial forces were applied to the models. For the CHS stub columns, fixed end support conditions were adopted as shown in Fig. 1 (a) by restraining all the rotations at the reference nodes (i.e.  $r_x = r_y = r_z = 0$ ), while the rotation about z axis was enabled in the finite element models of CHS long columns (i.e.  $r_x = r_y = 0$  but  $r_z \neq 0$ ), thereby establishing pin-end support conditions about z axis. Thus, the finite element models of CHS columns exhibited

global buckling behaviour about z axis for all the cases in this study which is appropriate considering the symmetry conditions adopted in the models as shown in Fig. 1 (b).

#### 2.4. Initial imperfections

While only local geometric imperfections were included in the finite element models of CHS stub columns, both local and global geometric imperfections were incorporated into the finite element models of CHS long columns. The lowest elastic local buckling modes obtained from the Linear Buckling Analyses (LBA) of the finite element models but with a modified thickness of  $t_{mod} = D/5$  were adopted to represent the local geometric imperfection shapes in the finite element models, thereby avoiding unrealistic, short buckling wavelengths in the definition of the local imperfections for CHS members with high  $D/t$  ratios. The same approach in the definition of local imperfections for tubular members has also been adopted in similar studies [44, 55] focused on the local buckling response of circular hollow and elliptical hollow section steel members, where its appropriateness and reliability have been verified. Moreover, for high-strength and normal-strength steel CHS members with practical proportions, the lowest eigenmode affine local imperfection shape approach has been used in a number of different studies in the literature [56–58] and shown to provide reliable estimations of their local buckling response. The local imperfection magnitudes were taken as equal to 80% of the fabrication tolerance of  $\omega_{local} = D/100$  provided in EN 10210 [20] for hot-finished circular hollow sections in line with the recommendations of EN 1993-1-5 [59] for the consideration of geometric imperfections in the finite element modelling of steel structures. For the case of global imperfections used for CHS long columns, the lowest global buckling modes from the LBA of the finite element models were used, which were scaled to 1/1000 of the member lengths (i.e.  $\omega_{global} = L/1000$ ). Residual stresses were not incorporated into the finite element models considering that their magnitudes are quite low within hot-finished CHS steel members, which assume even smaller values at elevated temperatures due to the development of thermal strains which leads to considerable reductions in the magnitudes of residual stresses.

#### 2.5. Validation of finite element models

In this subsection, the finite element modelling approach adopted in this paper is validated considering four experimental studies from the literature: (i) the fire experiments carried out on high-strength steel CHS columns by Tondini et al. [15], (ii) the experiments performed on high-strength steel CHS stub columns by Wei et al. [60] at room temperature, (iii) the fire experiments carried out on normal-strength steel CHS columns by Pires et al. [61] and (iv) the experiments performed on normal-strength steel CHS stub columns by O’Shea and Bridge [62] at room temperature.

##### 2.5.1. Tondini et al. [15] experiments on high-strength steel CHS columns

The experiments performed by Tondini et al. [15] on high-strength steel CHS columns in fire are utilised to validate the finite element modelling approach adopted in this paper herein. The experiments were carried out anisothermally, whereby a prescribed axial load was first applied to the specimens and then the temperature was increased until failure. The



geometrical properties of the specimens reported by [15] were included in the finite element models. The tested CHS specimens were made of high-strength steel with an average room temperature yield strength  $f_y$  of 822 MPa (i.e.  $f_y = 822$  MPa) and ultimate tensile strength  $f_u$  of 881 MPa (i.e.  $f_u = 881$  MPa), determined on the basis of the room temperature material tests performed on the coupons extracted from the tested specimens by [15]. The cross-sections of all the specimens fall into the Class 4 category according to EN 1993-1-2 [21], indicating that they are susceptible to both local and global instability effects. Since elevated temperature material tests were not carried out for the specimens by Tondini et al. [15], the 0.2% proof strength  $k_{p0.2,\theta}$ , Young's modulus  $k_{E,\theta}$ , ultimate strength  $k_{u,\theta}$  and ultimate strain  $k_{\epsilon_{u,\theta}}$  reduction factors determined by Qiang et al. [54] for S690 steel and shown in Table 1 were multiplied by the corresponding room temperature yield strength  $f_y$  and the ultimate strength  $f_u$  and strain  $\epsilon_u$  of the specimens measured by [15] to determine their elevated temperature values (i.e.  $f_{p0.2,\theta} = k_{p0.2,\theta}f_y$ ,  $f_{u,\theta} = k_{u,\theta}f_u$  and  $\epsilon_{u,\theta} = k_{\epsilon_{u,\theta}}\epsilon_u$ ), which were used in the finite element models. Note that even though the specimens of [15] were made of S590 steel, the measured room temperature yield and ultimate strengths were much higher than the mill certificate values and close to the room temperature yield strength and ultimate tensile strength values measured for coupons made of grade S690 steel by [53]; thus, the use of the material reduction factors derived by Qiang et al. [53] was found appropriate herein. The elevated temperature material stress-strain response was defined using eq. (3) in the finite element models, where the Ramberg-Osgood exponents  $n_\theta$  and  $m_\theta$  were determined using eq. (5). The temperature versus time relationships measured during the tests by Tondini et al. [15] were adopted in the finite element simulations; horizontal thermal gradients within the specimens reported by [15] owing to the presence of a furnace wall with gas burners on one side and a closing wall on the other side of the specimens were considered.

The axial deformation versus time paths of the specimens measured during the experiments and obtained from the finite element models created in this paper are shown in Fig. 5. As can be seen from the figure, the agreement between the experimentally and numerically determined axial deformation versus time paths is very good, indicating that the finite element models created in this study are able to replicate the response of high-strength steel CHS columns at elevated temperatures. The failure mode of the C1 specimen observed following the experiment of [15] and that observed in the finite element simulation carried out in this paper are compared in Fig. 6, where it can be seen that the failure mode observed in the numerical simulation is very similar to that observed in the experiment, thus providing a further verification for the accuracy of the finite element modelling approach adopted in this study with respect to the consideration of the structural response of CHS steel columns in fire.

In addition to the finite element models where the elevated temperature stress-strain response was defined using the two-stage elevated temperature material model of Fang and Chan [17, 51], the finite element models of the specimens were also created with the elevated temperature stress-strain relationships defined on the basis of the EN 1993-1-2 [21] elevated temperature material model with the yield strength  $k_{y,\theta}$  and Young's modulus reduction factors  $k_{E,\theta}$  given in EN 1993-1-2 [21]. Fig. 5 shows the axial deformation versus time paths

obtained through the finite element models with the EN 1993-1-2 [21] elevated temperature material model. As can be seen from the figure, the finite element models adopting the EN 1993-1-2 [21] elevated temperature material model generally provide structural response that is more favourable than that observed for the specimens in the experiments. Particularly, for the case of the C1 specimen, the use of the EN 1993-1-2 [21] elevated temperature material model leads to a significantly unconservative prediction of the structural behaviour, signifying that the adoption of the elevated temperature material model put forward by Fang and Chan [17, 51] as done in this study leads to more accurate and conservative predictions of the structural response of high-strength steel columns in fire.

### 2.5.2. *Wei et al. [60] experiments on high-strength steel CHS stub columns*

In addition to the fire tests performed on high-strength steel CHS columns by Tondini et al. [15], the experiments carried out on high-strength steel CHS stub columns at room temperature are also used in this paper for the validation of the adopted finite element modelling approach. Since there is no fire experiments performed on high-strength steel CHS stub columns, the room temperature CHS stub column tests of [60] are used for the validation herein. The CHS stub columns tested by Wei et al. [60] had an average 0.2% proof strength  $f_{p0.2}$  of 475 MPa. The geometric and material properties and material stress-strain response of the tested specimens reported in [60] were adopted in the finite element models created herein. Moreover, the geometric imperfections were applied to the finite element models as described in Section 2.4. Fig. 7 shows a comparison of the axial stress versus axial strain paths of the specimens measured during the experiments and those obtained from the finite element models created herein. As can be seen from the figure, the agreement between the experimental and numerical results is very good for CHS stub columns with both outer diameters of  $D = 64$  mm and  $D = 102$  mm and different ratios of  $D/t$ , thus verifying that the finite element models created in this study are able to consider the influence of local instabilities on the response of high-strength steel CHS members accurately.

### 2.5.3. *Pires et al. [61] experiments on normal-strength steel CHS columns*

In Pires et al. [61], a series of fire experiments were carried out on normal-strength steel CHS columns with axial and rotational restraints at the ends, which were also reported in [63]. The columns were made of grade S355 steel and the rotational restraints were provided against the rotations with respect to the two principal axes of the cross-sections of the specimens at the member ends. In the tests, for some specimens, the magnitudes of the axial restraint  $k_{\Delta}$  was equal to 13 kN/mm and those of the rotational restraints  $k_{\phi,1}$  and  $k_{\phi,2}$  with respect to the two principal axes of the column cross-sections were equal to 1992 kN/mm and 4091 kN/mm (i.e.  $k_{\Delta} = 13$  kN/mm,  $k_{\phi,1} = 1992$  kN/mm and  $k_{\phi,2} = 4091$  kN/mm); while for the others, the magnitudes of the axial restraint  $k_{\Delta}$  was equal to 128 kN/mm and those of the rotational restraints  $k_{\phi,1}$  and  $k_{\phi,2}$  with respect to the two principal axes of the column cross-sections were equal to 2536 kN/mm and 5079 kN/mm (i.e.  $k_{\Delta} = 128$  kN/mm,  $k_{\phi,1} = 2536$  kN/mm and  $k_{\phi,2} = 5079$  kN/mm). The tested columns had a length of 3 m, though only the middle portion of the columns with a length of 2.5 m was placed into the furnace, which resulted in thermal gradients along the lengths of the specimens.

The experiments were carried out anisothermally, whereby a prescribed axial load was first applied to the specimens and then the temperature was increased until failure. In the finite element models of the specimens created in this study, the EN 1993-1-2 [21] elevated temperature material model was used and the elevated temperature material properties of the specimens were determined by multiplying their room temperature material properties reported in [61] by the material strength and stiffness reduction factors provided in EN 1993-1-2 [21]. Time versus temperature relationships of the specimens reported in [61, 63] were taken into consideration in the anisothermal finite element simulations carried out herein.

The axial deformation versus time paths of the specimens observed during the experiments of [61] and those determined using the finite element models of the specimens created in this study are compared in Fig. 8 for the specimens with an outer diameter  $D$  of 219.1 mm and thickness  $t$  of 6 mm. As can be seen from the figure, there is a good agreement between the axial deformation versus time response of the specimens observed in the experiments and those obtained through the finite element models for different values of axial loading  $N_{Ed}$ , axial stiffness  $k_{\Delta}$  and rotational stiffness  $k_{\phi,1}$  and  $k_{\phi,2}$ , indicating that the finite element models created in this study are able to replicate the structural response of normal-strength steel columns in fire.

#### 2.5.4. O’Shea and Bridge [62] experiments on normal-strength steel CHS stub columns

O’Shea and Bridge [62] carried out a number of experiments on normal-strength steel CHS stub columns, which are used herein for the validation of the finite element modelling approach adopted in this study. The specimens had an outer diameter  $D$  of 165 mm and 190 mm with varying outer diameter-to-thickness  $D/t$  ratios. The geometric and material properties of the specimens reported in [62] were adopted in the finite element models created in this paper. The geometric imperfections were applied to the finite element models as described in Section 2.4. In Fig. 9, the axial stress  $\sigma$  normalised by the yield (i.e. 0.2% proof) strength  $f_y$  (i.e.  $\sigma/f_y$ ) versus axial strain  $\epsilon$  paths of the specimens obtained from the experiments of O’Shea and Bridge [62] and the finite element models developed in this study are compared. As can be seen from the figure, the finite element models created in this study provides axial stress versus strain paths that are in a good agreement with those observed in the experiments, which proves that the finite element models created in this study are able to account for the influence of local instability effects on the behaviour of normal-strength steel CHS stub columns accurately.

### 3. Parametric studies

With the aim of carrying out a comprehensive investigation into the accuracy of the existing rules in EN 1993-1-2 [21] for the design of high-strength steel and normal-strength steel CHS columns in fire and establishing new design methods leading to accurate and safe predictions of axial resistances of CHS steel members at elevated temperatures, extensive numerical parametric studies are carried out in this paper. A summary of the parametric studies performed in this paper is provided in Table 3. As can be seen from the table, for the case of CHS stub columns whose lengths  $L$  were taken as three times of their outer diameters

$D$  (i.e.  $L/D = 3$ ), (i) twenty outer cross-section diameter  $D$  to cross-section thickness  $t$  ratios (i.e.  $D/t$ ) ranging between 10 and 200 with increments in  $D/t$  of 10, (ii) five steel grades S690, S460, S355, S275 and S235 and (iii) five elevated temperature levels 300 °C, 400 °C, 500 °C, 600 °C and 700°C were considered, which all corresponded to the analyses of 500 CHS stub columns in total. In the case of CHS long columns, (i) ten member length  $L$  to outer cross-section diameter  $D$  ratios  $L/D$  ranging between 5 and 50 with increment in  $L/D$  of 5, (ii) five outer cross-section diameter  $D$  to thickness  $t$  ratios  $D/t$  equal to 25, 50, 100, 150 and 200, (iii) five steel grades S690, S460, S355, S275 and S235 and (iv) five elevated temperature levels 300 °C, 400 °C, 500 °C, 600 °C and 700°C were taken into account, resulting in the consideration of 1250 CHS columns. In the following section, the results from the extensive numerical parametric studies are used to assess the accuracy of EN 1993-1-2 [21] for the design of CHS members under axial compression in fire and in the development of new design proposals.

#### 4. Assessment of EN 1993-1-2 for axial compression resistance predictions of CHS steel members in fire

In this section, the design rules existing in EN 1993-1-2 [21] for the ultimate resistance predictions of CHS members under axial compression in fire are set out, which are then assessed against the results obtained from the Geometrically and Materially Nonlinear Analyses with Imperfections (GMNIA) of the finite elements models of CHS members at elevated temperatures. In the following section, the design rules proposed in this paper, which provide more accurate ultimate axial compression resistance predictions of CHS members in fire, are introduced.

##### 4.1. Design rules provided in EN 1993-1-2 for the determination of axial compression resistances of CHS steel members in fire

According to EN 1993-1-2 [21], the design buckling resistance  $N_{b,fi,t,Rd}$  at time  $t$  of a compression member with a uniform temperature  $\theta$  is determined using the following expressions:

$$\begin{aligned} N_{b,fi,t,Rd} &= \frac{\chi_{fi} A k_{y,\theta} f_y}{\gamma_{M,fi}} \quad \text{for} \quad \frac{D}{t} \leq 90\epsilon_\theta^2, \\ N_{b,fi,t,Rd} &= \frac{\chi_{fi} A_{eff} k_{p0.2,\theta} f_y}{\gamma_{M,fi}} \quad \text{for} \quad \frac{D}{t} > 90\epsilon_\theta^2, \end{aligned} \quad (7)$$

where  $A$  is the full cross-section area used for CHS members with Class 1, 2 and 3 sections (i.e. sections with  $D/t \leq 90\epsilon_\theta^2$ ),  $A_{eff}$  is the effective cross-section area used for CHS members with Class 4 sections (i.e. sections with  $D/t > 90\epsilon_\theta^2$ ),  $\gamma_{M,fi}$  is the partial safety factor taken as equal to unity and  $\epsilon_\theta$  is the elevated temperature material constant calculated by the multiplication of the room temperature material constant  $\epsilon$  by a factor of 0.85 as given below

$$\epsilon_\theta = 0.85\epsilon = 0.85\sqrt{\frac{235}{f_y}}. \quad (8)$$

As can be seen from eq. (7), while EN 1993-1-2 [21] recommends the use of the elevated temperature material strength at 2% total strain  $f_{y,\theta} = k_{y,\theta}f_y$  for CHS members with Class 1, 2 and 3 sections, it recommends the use of the elevated temperature 0.2% proof strength  $f_{p0.2,\theta} = k_{p0.2,\theta}f_y$  for those with Class 4 sections. Note that the Class 4  $D/t$  limit ratios are 22.1, 33.2 and 43.0 for members made of steels with yield strengths of 690 MPa, 460 MPa and 355 MPa, respectively. In eq. (7),  $\chi_{fi}$  is the column buckling reduction factor determined as

$$\chi_{fi} = \frac{1}{\phi_\theta + \sqrt{\phi_\theta^2 - \bar{\lambda}_\theta^2}} \quad (9)$$

with

$$\phi_\theta = 0.5 \left[ 1 + \alpha \bar{\lambda}_\theta + \bar{\lambda}_\theta^2 \right] \quad (10)$$

and

$$\alpha = 0.65 \sqrt{235/f_y}. \quad (11)$$

The non-dimensional slenderness  $\bar{\lambda}_\theta$  for the temperature  $\theta$  is given by

$$\bar{\lambda}_\theta = \bar{\lambda} \sqrt{\frac{k_{y,\theta}}{k_{E,\theta}}}, \quad (12)$$

where  $\bar{\lambda}$  is non-dimensional slenderness at room temperature determined as

$$\begin{aligned} \bar{\lambda} &= \sqrt{\frac{Af_y}{N_{cr}}} \quad \text{for} \quad \frac{D}{t} \leq 90\epsilon_\theta^2, \\ \bar{\lambda} &= \sqrt{\frac{A_{eff}f_y}{N_{cr}}} \quad \text{for} \quad \frac{D}{t} > 90\epsilon_\theta^2, \end{aligned} \quad (13)$$

in which  $N_{cr}$  is the elastic global flexural buckling load of a CHS member at room temperature.

For the case of Class 4 CHS members, EN 1993-1-2 [21] directs the designer to the room temperature structural steel design standard EN 1993-1-1 [22] for the determination of the effective cross-section area  $A_{eff}$ , for which EN 1993-1-1 [22] recommends the use of the relevant design rules provided in EN 1993-1-6 [23]. Since the reduction in the cross-section strength of CHS columns is characterised by the ultimate-to-yield stress ratio  $\rho = f_u/f_y$  in EN 1993-1-6 [23], the concept of a loss of effectiveness can be utilised as the basic design approach as recommended by [55], whereby the effective area of a Class 4 CHS member can be determined as:

$$\rho = \frac{f_u}{f_y} = \frac{A_{eff}}{A}. \quad (14)$$

The existing provisions of EN 1993-1-6 [23] recommend the following expressions for the determination of a local buckling reduction factor  $\rho$  for a Class 4 CHS member subjected to axial compression:

$$\rho = \begin{cases} 1 & \text{for } \bar{\lambda}_l \leq 0.2 \\ 1 - \beta_{pl} \left( \frac{\bar{\lambda}_l - 0.2}{\bar{\lambda}_p - 0.2} \right)^\eta & \text{for } 0.2 < \bar{\lambda}_l < \bar{\lambda}_p \\ \alpha_{el} / \bar{\lambda}_l^2 & \text{for } \bar{\lambda}_l \geq \bar{\lambda}_p \end{cases} \quad (15)$$

in which  $\bar{\lambda}_l$  is the non-dimensional local buckling slenderness defined by

$$\bar{\lambda}_l = \sqrt{\frac{f_y}{f_{cr}}}, \quad (16)$$

where  $f_{cr}$  is the elastic critical local buckling stress of a CHS member which is determined as:

$$f_{cr} = \frac{E}{\sqrt{3(1-\nu^2)}} \frac{2t}{D}. \quad (17)$$

In eq. (15),  $\alpha_{el}$  is the elastic buckling reduction factor calculated as:

$$\alpha_{el} = \frac{0.83}{1 + 2.2 (\omega_{local}/t)^{0.88}}, \quad (18)$$

$\beta_{pl}$  is the plastic range factor given by

$$\beta_{pl} = 1 - \frac{0.95}{1 + 1.2 (\omega_{local}/t)}, \quad (19)$$

and  $\eta$  is the interaction exponent determined using the following expression:

$$\eta = \frac{5.4}{1 + 4.6 (\omega_{local}/t)}. \quad (20)$$

The plastic limit relative slenderness used in eq. (15) can be determined from:

$$\bar{\lambda}_p = \sqrt{\frac{\alpha_{el}}{1 - \beta_{pl}}}. \quad (21)$$

Note that eqs. (18), (19) and (20) used for the determination of  $\alpha_{el}$ ,  $\beta_{pl}$  and  $\eta$  were taken from Annex D of EN 1993-1-6 [23]; the derivation of these equations are described in [64–66]. In the following subsection, the accuracy of EN 1993-1-2 [21] for the assessment of structural response of CHS members under axial compression in fire is explored considering a broad range of parameters summarised in Section 3.

#### 4.1.1. Accuracy of EN 1993-1-2 for the determination of axial compression resistances of CHS steel members in fire

The accuracy of the existing provisions of EN 1993-1-2 [21] for the ultimate strength predictions of CHS stub columns in fire is illustrated in Fig. 10 for different elevated temperature levels, local buckling slendernesses and steel grades. Note that since global member imperfections were not incorporated into the finite element models of CHS stub columns, the global buckling reduction factor  $\chi_{fi}$  was taken as equal to unity in eq. (7) in the determination of the axial compression resistances according to EN 1993-1-2 [21]. In Fig. 10, the cross-sections are classified as Class 4 if their outer diameter to thickness ratios  $D/t$  are greater than  $90\epsilon_\theta^2$  (i.e.  $D/t > 90\epsilon_\theta^2$ ). Fig. 10 shows that EN 1993-1-2 [21] provides quite inaccurate estimations of the cross-section axial compression resistances of CHS columns in fire. As can be seen from the figure, the use of the elevated temperature material strengths at 2% strain  $f_{y,\theta} = k_{y,\theta}f_y$  for Class 1, 2 and 3 sections and the elevated temperature 0.2% proof strengths  $f_{p0.2,\theta} = k_{p0.2,\theta}f_y$  for Class 4 sections results in a discontinuity in the predictions of the cross-section axial compression resistances, with significant underpredictions of the ultimate resistances of Class 4 CHS stub columns in fire. The multiple resistance prediction curves of EN 1993-1-2 [21] for different elevated temperature levels shown in Fig. 10 in the case of Class 4 sections (i.e. for  $D/t > 90\epsilon_\theta^2$ ) result from different ratios of the elevated temperature 0.2% proof strengths  $f_{p0.2,\theta} = k_{p0.2,\theta}f_y$  to yield strengths  $f_{y,\theta} = k_{y,\theta}f_y$  (i.e.  $f_{p0.2,\theta}/f_{y,\theta}$ ) at different elevated temperature levels.

Fig. 10 also shows that relative to the elevated temperature axial compression resistances of normal-strength grade S355 and S235 steel CHS stub columns, those of high-strength steel grade S690 and S460 stub columns exhibit a higher level of scatter; for the latter, EN 1993-1-2 [21] leads to a lower degree of accuracy. The higher scatter in the ultimate strengths of high-strength steel CHS stub columns was attributed to (i) the change of the roundedness of the elevated temperature stress-strain response for high-strength steels at different temperature levels with different  $n_\theta$  and  $m_\theta$  exponents unlike the same level of roundedness of the elliptical EN 1993-1-2 [21] stress-strain curve adopted for normal-strength steels for all elevated temperature levels, (ii) rather significantly varying ratios of the elevated temperature 0.2% proof strengths  $f_{p0.2,\theta} = k_{p0.2,\theta}f_y$  to ultimate strengths  $f_{u,\theta} = k_{u,\theta}f_u$  (i.e.  $f_{p0.2,\theta}/f_{u,\theta}$ ) for different temperature levels, which are closer to unity in some cases as can be seen from Table 1 and Table 2; CHS members lose their initial elevated temperature stiffness at later stages of the loading history for high  $f_{p0.2,\theta}/f_{u,\theta}$  ratios which leads to larger ultimate cross-section resistances and (iii) the use of the elevated temperature strength at 2% strain  $f_{y,\theta} = k_{y,\theta}f_y$  in the normalisation of the axial compression resistances even though in some cases the strains  $\epsilon_{u,\theta}$  corresponding to the elevated temperature ultimate material strengths  $f_{u,\theta} = k_{u,\theta}f_u$  were lower than 2% for grade S690 and S460 steels as shown in Fig. 4. Since in some instances the elevated temperature strengths at 2% total strain  $f_{y,\theta} = k_{y,\theta}f_y$  are located within the descending branch of the elevated temperature stress-strain curves of high-strength steels (see Fig. 4), it may be argued that the use of  $f_{y,\theta} = k_{y,\theta}f_y$  in the determination of the ultimate resistances of high strength steel members in fire may not be appropriate for these cases. This is because the ultimate load carrying capacities of CHS members are primarily influenced by the parts of the stress-strain curves up to the elevated

temperature ultimate tensile strengths  $f_{u,\theta} = k_{u,\theta} f_y$ .

In addition to the assessment of cross-section axial compression resistance predictions of EN 1993-1-2 [21] for CHS stub columns at elevated temperatures, the accuracy of EN 1993-1-2 [21] for the predictions of flexural buckling resistances of CHS columns in fire is also assessed in Fig. 11, considering different cross-section outer diameter to thickness ratios  $D/t$ , non-dimensional slendernesses  $\bar{\lambda}_\theta$  and elevated temperature levels. Note that in Fig. 11,  $A^*$  is equal to the full cross-section area  $A$  for Class 1, 2 and 3 sections (i.e.  $A^* = A$  for Class 1, 2 and 3 sections) and equal to the effective cross-section area  $A_{eff}$  for Class 4 sections (i.e.  $A^* = A_{eff}$  for Class 4 sections). As can be seen from Fig. 11, due primarily to the inaccurate predictions of the cross-section axial compression resistances, EN 1993-1-2 [21] leads to quite inaccurate estimations of the ultimate strength predictions of CHS columns in fire, with generally significant underestimations of the ultimate resistances. It should however be noted that for the case Class 1, 2 and 3 CHS columns in fire, EN 1993-1-2 [21] considerably overestimates the ultimate resistances in some cases, which can be seen in Fig. 12 where the accuracy of EN 1993-1-2 [21] is assessed for CHS columns with Class 1, 2 and 3 sections.

As can be understood from the results presented in this section, the design rules existing in EN 1993-1-2 [21] lead to quite inaccurate predictions of the ultimate cross-section axial compression resistances and flexural buckling resistances of both high-strength steel and normal-strength steel CHS columns in fire, signifying the need for the development of design formulae leading to accurate estimations of the structural response of such members. In the following section, new design rules for the determination of cross-section axial compression resistances and flexural buckling resistances of CHS columns at elevated temperatures are put forward.

## 5. Proposed design rules for high-strength steel and normal-strength steel CHS steel columns in fire

To enable more accurate ultimate strength predictions of CHS steel members under axial compression in fire, new design rules are proposed in this section. Initially, the proposed design rules are introduced; then their accuracy for the determination of the axial compressive resistances of CHS stub columns and long columns at elevated temperatures is assessed against the results obtained from GMNIA. The accuracy and reliability of the proposed design rules are also compared against those of the existing design provisions of EN 1993-1-2 [21].

### 5.1. Proposed design rules for the determination of axial compression resistances of CHS steel members in fire

The design buckling resistance  $N_{b,fi,t,Rd}$  at time  $t$  of a compression member with a uniform temperature  $\theta$  is proposed to be determined using the following expressions:

$$N_{b,fi,t,Rd} = \frac{\chi_{fi} A k_{y,\theta}^* f_y}{\gamma_{M,fi}} \quad \text{for} \quad \bar{\lambda}_{l,\theta} \leq \bar{\lambda}_{l,\theta,0},$$



$$N_{b,fi,t,Rd} = \frac{\chi_{fi} A_{eff} k_{y,\theta}^* f_y}{\gamma_{M,fi}} \quad \text{for } \bar{\lambda}_{l,\theta} > \bar{\lambda}_{l,\theta,0}, \quad (22)$$

where  $\bar{\lambda}_{l,\theta}$  is the non-dimensional elevated temperature local buckling slenderness of a CHS section calculated as

$$\bar{\lambda}_{l,\theta} = \bar{\lambda}_l \sqrt{\frac{k_{y,\theta}^*}{k_{E,\theta}}} = \sqrt{\frac{f_y}{f_{cr}}} \sqrt{\frac{k_{y,\theta}^*}{k_{E,\theta}}}, \quad (23)$$

in which  $k_{y,\theta}^*$  is the modified elevated temperature yield strength factor determined as given below

$$\begin{aligned} k_{y,\theta}^* &= k_{y,\theta} & \text{if } k_{\epsilon_{u,\theta}} \epsilon_u \geq 0.02, \\ k_{y,\theta}^* &= k_{u,\theta} \frac{f_u}{f_y} & \text{if } k_{\epsilon_{u,\theta}} \epsilon_u < 0.02. \end{aligned} \quad (24)$$

This approach is recommended to avoid the use of the elevated temperature strengths at 2% (i.e.  $f_{y,\theta} = k_{y,\theta} f_y$ ) when the strain corresponding to the elevated temperature ultimate strength  $\epsilon_{u,\theta} = k_{\epsilon_{u,\theta}} \epsilon_u$  is smaller than 2% (i.e.  $\epsilon_{u,\theta} < 0.02$ ), which is observed for high-strength steels in some cases due to their reduced ductility relative to normal-strength steels (see Fig. 4), thereby preventing the use of material strengths within the descending branch of the stress-strain curves and using the elevated temperature ultimate tensile strengths  $f_{u,\theta} = k_{u,\theta} f_u$  in the determination of ultimate resistances for these cases. In eq. (22),  $\bar{\lambda}_{l,\theta,0}$  is the threshold non-dimensional local buckling slenderness; if the elevated temperature non-dimensional local buckling slenderness of a CHS  $\bar{\lambda}_{l,\theta}$  is greater than  $\bar{\lambda}_{l,\theta,0}$  (i.e.  $\bar{\lambda}_{l,\theta} > \bar{\lambda}_{l,\theta,0}$ ), it is classified as Class 4 and its effective section area  $A_{eff}$  is utilised in the determination of its axial compression resistance. It should be noted that unlike the existing design rules in EN 1993-1-2 [21], this study recommends the use of the same material strengths  $k_{y,\theta}^* f_y$  in the determination of the axial compression resistances of CHS members with sections falling into all Class 1, 2, 3 and 4 categories as can be seen from eq. (22). Since effective cross-section areas  $A_{eff}$  are used in the determination of the axial compression resistances of CHS columns with Class 4 sections and full cross-section areas  $A$  are used for the calculation of the ultimate load carrying capacities of those with Class 1, 2 and 3 sections, only the limit for the classification of a CHS as Class 4 is provided herein. Future research will be directed towards the behaviour of high-strength and normal-strength steel CHS members under bending and combined bending and axial compression in fire, for which new classification limits for Class 1, 2 and 3 sections will be developed.

In eq. (22), the column buckling reduction factor  $\chi_{fi}$  is determined as

$$\chi_{fi} = \frac{1}{\phi_\theta + \sqrt{\phi_\theta^2 - \bar{\lambda}_\theta^2}} \quad (25)$$

with

$$\phi_\theta = 0.5 \left[ 1 + \alpha \bar{\lambda}_\theta + \bar{\lambda}_\theta^2 \right] \quad (26)$$

and

$$\alpha = 0.90\sqrt{235/f_y}. \quad (27)$$

As can be seen from eq. (27), a higher imperfection factor  $\alpha = 0.90\sqrt{235/f_y}$  is recommended herein relative to  $\alpha = 0.65\sqrt{235/f_y}$ , which was obtained through calibration against the GMNIA results of long CHS columns with different elevated temperature levels, steel grades and length-to-cross-section diameter ratios  $L/D$  in this paper.

The effective cross-section area  $A_{eff}$  of a Class 4 section used in eq. (22) can be determined as

$$A_{eff} = \rho A. \quad (28)$$

Following equations are proposed for the determination of a reduction factor  $\rho$  used for the calculation of effective cross-section areas  $A_{eff}$  of CHS members, which were determined through calibration against GMNIA results of CHS stub columns with various outer diameter-to-thickness ratios  $D/t$  and different elevated temperature levels and steel grades:

$$\begin{aligned} \rho &= 1.0 & \text{for } \bar{\lambda}_{l,\theta} \leq \bar{\lambda}_{l,\theta,0}, \\ \rho &= 1 - \beta_\theta (\bar{\lambda}_{l,\theta} - \bar{\lambda}_{l,\theta,0}) & \text{for } \bar{\lambda}_{l,\theta} > \bar{\lambda}_{l,\theta,0}, \end{aligned} \quad (29)$$

where  $\beta_\theta$  is the auxiliary coefficient taken as

$$\beta_\theta = 0.8, \quad (30)$$

and  $\bar{\lambda}_{l,\theta,0}$  is the threshold slenderness calculated by

$$\bar{\lambda}_{l,\theta,0} = 0.4 - 0.2\sqrt{235/f_y}. \quad (31)$$

Note that the proposed expressions for the determination of  $\rho$  given by eq. (29) uses the elevated temperature local buckling slenderness  $\bar{\lambda}_{l,\theta} = \bar{\lambda}_l \sqrt{k_{y,\theta}^*/k_{E,\theta}}$  of a CHS, thereby considering the influence of the differential erosion rates of strength and stiffness on the local buckling response of CHS members under axial compression at elevated temperatures. Moreover, the proposed equations for the determination of the reduction factor  $\rho$  for the consideration of local buckling in CHS members in fire employs threshold slenderness  $\bar{\lambda}_{l,\theta,0}$  varying with the yield strength of steel as can be seen from eq. (31). The higher the yield strength, the longer the plateau slenderness  $\bar{\lambda}_{l,\theta,0}$  below which  $\rho$  is taken as equal to unity (i.e.  $\rho = 1.0$ ). This is in line with the observations made using the numerical benchmark data obtained for CHS stub columns at elevated temperatures in this paper. It should also be emphasised that as can be seen from eq. (22) and eq. (23), the use of the elevated temperature ultimate strengths  $f_{u,\theta}$  in lieu of the elevated temperature yield strengths  $f_{y,\theta}$  for the cases where  $\epsilon_{u,\theta} = k_{\epsilon_{u,\theta}} \epsilon_u < 0.02$  leads to an increase in the local buckling slenderness of a cross-section  $\bar{\lambda}_\theta$  by a factor of  $\sqrt{f_{u,\theta}/f_{y,\theta}}$ . Thus, a cross-section classified as Class 3

using the elevated temperature yield strength  $f_{y,\theta}$  can fall into a Class 4 category when the elevated temperature ultimate tensile strength  $f_{u,\theta}$  is used to determine its resistance and if the cross-section is not able to reach the ultimate load carrying capacity of  $N_{ult} = Af_{u,\theta}$ . This was taken into consideration in the calibration of the local buckling reduction factor  $\rho$  formulae and the threshold slenderness  $\bar{\lambda}_{l,\theta,0}$  expression provided in eq. (29) and eq. (31) by using the elevated temperature ultimate tensile strength  $f_{u,\theta}$  for cross-sections where  $\epsilon_{u,\theta} = k_{\epsilon_{u,\theta}}\epsilon_u < 0.02$ . In the following subsection, the accuracy of the new design proposals for the determination of the ultimate cross-section axial compression resistances and flexural buckling resistances of CHS members in fire is explored.

### 5.2. Assessment of the accuracy of the proposed design rules against the existing design rules in EN 1993-1-2

In this subsection, the accuracy of the proposed design method for the determination of the axial compression resistances of CHS members in fire is investigated. Fig. 13 illustrates the assessment of the ultimate axial compression resistances determined through the proposed method against those obtained from GMNIA for CHS stub columns with various elevated temperature cross-section local buckling slendernesses  $\bar{\lambda}_{l,\theta}$ , steel grades and elevated temperature levels. As can be seen from the figure, the proposed approach leads to considerably more accurate ultimate cross-section axial compression resistance predictions relative to EN 1993-1-2 [21] for CHS members in fire. The use of a single reference material strength  $f_{y,\theta} = k_{y,\theta}^*f_y$  in the proposed method precludes the discontinuity in the resistance predictions made for Class 4 and Class 1, 2 and 3 sections, thereby resulting in a much more accurate assessment of the behaviour relative to EN 1993-1-2 [21]. The proposed approach is particularly very accurate for normal-strength grade S355, S275 and S235 CHS members, though it also leads to safe and accurate strength predictions for high strength steel grade S690 and S460 steel CHS members. Note that the conservative predictions for high-strength grade S690 and S460 steel CHS stub columns were primarily observed for the cases where the ratios of the elevated temperature 0.2% proof strengths  $f_{p0.2,\theta} = k_{p0.2,\theta}f_y$  to ultimate tensile strengths  $f_{u,\theta} = k_{u,\theta}f_y$  (i.e.  $f_{p0.2,\theta}/f_{u,\theta}$ ) are high, which can be understood by comparing the strength reduction factors  $k_{p0.2,\theta}$  and  $k_{u,\theta}$  provided in Tables 1 and 2 with the results presented in Fig. 13 (a) and (b). As previously stated, in the cases where  $f_{p0.2,\theta}/f_{u,\theta}$  ratios are high, the CHS stub columns lose their initial elevated temperature stiffness at later stages of the loading history relative to those with low  $f_{p0.2,\theta}/f_{u,\theta}$  ratios, thus exhibiting higher local buckling strengths at elevated temperatures. For the case of normal-strength grade S355, S275 and S235 steel CHS stub columns, since (i) the ratios of the elevated temperature proof strengths  $f_{p,\theta} = k_{p,\theta}f_y$ , after which the material starts to lose its initial elevated temperature stiffness as can be seen from Fig. 2, to the elevated temperature strengths at 2% total strain  $f_{y,\theta} = k_{y,\theta}f_y$  (i.e.  $f_{p,\theta}/f_{y,\theta}$ ) are rather constant in the practical elevated temperature range of 300 °C – 700 °C and (ii) the same elliptical material model was assumed for different temperatures, similar local buckling response at different elevated temperature levels was observed. This enables the very accurate local buckling strength estimations of the proposed method for all the considered parameters in the case of normal-strength CHS stub columns as can be seen from Fig. 13.

A statistical appraisal of the accuracy of the proposed design approach for the determination of the ultimate elevated temperature cross-section axial compression resistances of CHS members against that of EN 1993-1-2 [21] is provided in Table 4, where  $N$  is the number of the considered stub columns,  $\epsilon$  is the ratio of the ultimate resistance of a stub column obtained from GMNIA to that determined through a design method (i.e.  $\epsilon = R_{GMNIA}/R_{method}$ ) and  $\epsilon_{av}$ ,  $\epsilon_{COV}$ ,  $\epsilon_{max}$  and  $\epsilon_{min}$  are the average, coefficient of variation, maximum and minimum of  $\epsilon$  values respectively. As can be seen from Table 4, relative to EN 1993-1-2 [21], the proposed approach leads to significantly more accurate ultimate cross-section resistance predictions of both high-strength steel and normal-strength steel CHS columns in fire. The accuracy of the proposed design approach relative to EN 1993-1-2 [21] is also graphically illustrated in Fig. 14, where the considerably higher accuracy of the proposed design method can also be observed.

Following the assessment of the accuracy of the proposed design approach for the cross-section axial compression resistances of CHS members in fire, its accuracy for the predictions of the flexural buckling strengths of CHS columns at elevated temperatures is also investigated in Fig. 15. As can be seen from the figure, the proposed design method leads to safe and accurate flexural buckling strength predictions for different steel grades, slendernesses  $\bar{\lambda}_\theta$  and elevated temperature levels. The accuracy of the proposed design approach is assessed in Fig. 16 for the ultimate strength predictions of CHS columns with Class 1, 2 and 3 sections in fire. Comparing Fig. 16 with Fig. 12, it can be observed that the use of the imperfection factor expression given in eq. (27) relative to the EN 1993-1-2 [21] imperfection factor expression provided in eq. (11) results in safer ultimate strength predictions for CHS columns with Class 1, 2 and 3 sections in fire. In Table 5, the accuracy of the proposed design method is also compared against that of EN 1993-1-2 [21]. As can be seen from the table, the proposed design method leads to more accurate and safe ultimate strength predictions relative to EN 1993-1-2 [21] for high-strength and normal-strength steel CHS columns in fire with lower  $\epsilon_{COV}$  ratios. The relatively higher accuracy of the proposed design method against EN 1993-1-2 [21] for ultimate strength predictions of CHS columns in fire is also graphically shown in Fig. 17. For the purpose of investigating the accuracy of the use of the imperfection factor  $\alpha = 0.65\sqrt{235/f_y}$  recommended in EN 1993-1-2 [21] in the proposed design method, the ratios of the ultimate resistances obtained from GMNIA to those determined by using  $\alpha = 0.65\sqrt{235/f_y}$  in lieu of  $\alpha = 0.90\sqrt{235/f_y}$  in eq. (22) are also provided in Table 5, where it can be seen that the use of  $\alpha = 0.65\sqrt{235/f_y}$  in the proposed design method leads to somewhat unsafe results in some cases. However, note that the imperfection factor  $\alpha = 0.65\sqrt{235/f_y}$  adopted in EN 1993-1-2 [21] was developed considering the ultimate resistances of normal-strength steel columns obtained from a large number of fire experiments [24], where the likelihood of specimens having the imperfection magnitude of  $\omega_{global} = L/1000$  with the most detrimental imperfection shape (i.e. in the shape of the lowest buckling mode) is small; the original imperfection factor recommended for EN 1993-1-2 [21] considering the worst geometric imperfection shape with a magnitude of  $\omega_{global} = L/1000$  was higher [24]. Thus, a comprehensive number of fire experiments that will be carried out on high-strength steel CHS columns may indicate the suitability of the

use of an imperfection factor expression providing imperfection factors smaller than those obtained through the imperfection factor expression of  $\alpha = 0.90\sqrt{235/f_y}$  proposed in this study.

Finally, the reliability of the proposed design method for the design of CHS columns at elevated temperatures is assessed in Table 6 taking into consideration the three reliability criteria proposed by Kruppa [67] for the design of steel members in fire. Note that the three reliability criteria proposed by Kruppa [67] have been approved and adopted by the CEN TC/250 Horizontal Group focusing the development of the European structural steel fire design standard EN 1993-1-2 [21] for the assessment of the accuracy and reliability of methods for the fire design of steel structures, which were also used in [68–71]. According to Criterion 1 of [67], none of the strength predictions obtained through the considered design approach should exceed GMNIA results by more than 15%, while Criterion 2 states that less than 20% of the design predictions should be on the unsafe side. Finally, Criterion 3 states that the design predictions should be safe-sided on average. In Table 6, the percentage of the columns for which the overestimations of the ultimate strengths exceeded 15% of those obtained from GMNIA is shown under Criterion 1, the percentage of the columns whose ultimate resistances were overestimated is shown under Criterion 2 and the average percentage of the differences between the design and GMNIA ultimate strengths is shown under Criterion 3. The violated criteria are highlighted with ‘\*’. As can be seen from Table 6, the proposed method satisfies all the reliability criteria of Kruppa [67] with the exception of Criterion 2 but this is deemed to be acceptable considering that Criterion 1 is only violated for a small number of very slender CHS columns with  $\bar{\lambda}_\theta > 2.0$  which are generally outside of the column proportions used in practice. On the other hand, Table 6 shows that EN 1993-1-2 [21] generally violates the reliability criteria of Kruppa [67], proving that the proposed design method leads to both more reliable and accurate ultimate strength predictions of high-strength and normal-strength CHS columns at elevated temperatures. The reliability of the proposed design method is also assessed in Table 6 when it is used with the imperfection factor expression  $\alpha = 0.65\sqrt{235/f_y}$  recommended in EN 1993-1-2 [21], where it can be seen that it leads to the violation of a number of reliability criteria recommended by Kruppa [67].

## 6. Conclusions

In this paper, the behaviour and design of high-strength and normal-strength grade S690, S460, S355, S275 and S235 steel CHS members subjected to axial compression in fire is investigated. Finite element models of CHS steel members were created and validated against the results obtained from experiments on CHS steel columns in fire and room temperature. Following the validation of the finite element models, they were utilised to carry out extensive numerical parametric studies to generate comprehensive structural performance data for CHS stub columns and long columns at elevated temperatures, considering different steel grades, elevated temperature levels, local cross-section slenderness and global member slenderness. In total, 500 CHS stub columns and 1250 long CHS columns were considered in the numerical parametric studies. The obtained structural performance data of CHS members

subjected to axial compression in fire were then used to assess the existing provisions of EN 1993-1-2 [21] for the determination of cross-section axial compression resistances and flexural buckling resistances of CHS columns at elevated temperatures. It was observed that EN 1993-1-2 [21] leads to quite inaccurate predictions of the ultimate cross-section axial compression resistances and flexural buckling resistances of CHS steel columns susceptible to local and global buckling effects in fire, where the predictions were particularly more inaccurate for high strength steel CHS members. For the purpose of establishing a more accurate way of assessing the structural response of CHS columns at elevated temperatures, a new design method for the determination of the axial compression resistances of CHS members in fire was put forward. It was illustrated that the proposed method leads to considerably more accurate and safe cross-section axial compression resistances and flexural buckling resistances of both high-strength and normal-strength CHS columns influenced by local and global instability effects at elevated temperatures. The reliability of the proposed design method was also verified using the three reliability criteria set out by Kruppa [67] for the design of structural steel members in fire, while the existing design rules in EN 1993-1-2 [21] violated a number of reliability criteria of [67] for CHS columns at elevated temperatures. In this paper, the cross-section axial compression resistances and flexural buckling resistances of high-strength and normal-strength steel grade S690, S460, S355, S275 and S235 CHS members in fire were investigated, future research will be directed towards the behaviour and design of high-strength and normal-strength steel CHS members under bending and combined bending and axial compression at elevated temperatures. Future research will also focus on the structural response and design of high-strength and normal-strength tubular steel members with square, rectangular and elliptical hollow sections in fire.

## References

- [1] EN 1993-1-12, Eurocode 3 Design of steel structures-Part 1-12: Additional rules for the extension of EN 1993 up to steel grades S 700. European Committee for Standardization (CEN), Brussels; 2007.
- [2] Standards Australia, AS 4100 steel structures. Australian Building Codes Board, Sydney; 1998.
- [3] Rasmussen, K.J., Hancock, G.J.. Tests of high strength steel columns. *Journal of Constructional Steel Research* 1995;34(1):27–52.
- [4] Yang, D., Hancock, G.J.. Numerical simulation of high-strength steel box-shaped columns failing in local and overall buckling modes. *Journal of Structural Engineering, ASCE* 2006;132(4):541–549.
- [5] Shi, G., Ban, H., Bijlaard, F.S.. Tests and numerical study of ultra-high strength steel columns with end restraints. *Journal of Constructional Steel Research* 2012;70:236–247.
- [6] Wang, Y.B., Li, G.Q., Chen, S.W., Sun, F.F.. Experimental and numerical study on the behavior of axially compressed high strength steel columns with H-section. *Engineering Structures* 2012;43:149–159.
- [7] Ban, H., Shi, G., Shi, Y., Bradford, M.A.. Experimental investigation of the overall buckling behaviour of 960 MPa high strength steel columns. *Journal of Constructional Steel Research* 2013;88:256–266.
- [8] Yoo, J.H., Kim, J.W., Yang, J.G., Kang, J.W., Lee, M.J.. Local buckling in the stub columns fabricated with HSA800 of high performance steel. *International Journal of Steel Structures* 2013;13(3):445–458.
- [9] Wang, Y.B., Li, G.Q., Chen, S.W., Sun, F.F.. Experimental and numerical study on the behavior of axially compressed high strength steel box-columns. *Engineering Structures* 2014;58:79–91.
- [10] Shi, G., Zhou, W., Bai, Y., Lin, C.. Local buckling of 460 MPa high strength steel welded section stub columns under axial compression. *Journal of Constructional Steel Research* 2014;100:60–70.

- [11] Ma, J.L., Chan, T.M., Young, B.. Experimental investigation on stub-column behavior of cold-formed high-strength steel tubular sections. *Journal of Structural Engineering*, ASCE 2015;142(5):04015174.
- [12] Li, T.J., Li, G.Q., Chan, S.L., Wang, Y.B.. Behavior of Q690 high-strength steel columns: Part 1: Experimental investigation. *Journal of Constructional Steel Research* 2016;123:18–30.
- [13] Li, T.J., Liu, S.W., Li, G.Q., Chan, S.L., Wang, Y.B.. Behavior of Q690 high-strength steel columns: Part 2: Parametric study and design recommendations. *Journal of Constructional Steel Research* 2016;122:379–394.
- [14] Chen, J., Young, B.. Design of high strength steel columns at elevated temperatures. *Journal of Constructional Steel Research* 2008;64(6):689–703.
- [15] Tondini, N., Rossi, B., Franssen, J.M.. Experimental investigation on ferritic stainless steel columns in fire. *Fire Safety Journal* 2013;62:238–248.
- [16] Winful, D., Cashell, K., Afshan, S., Barnes, A., Pargeter, R.. Behaviour of high strength steel columns under fire conditions. *Journal of Constructional Steel Research* 2018;150:392–404.
- [17] Fang, H., Chan, T.M.. Axial compressive strength of welded S460 steel columns at elevated temperatures. *Thin-Walled Structures* 2018;129:213–224.
- [18] Tenaris, High Strength Steel (HSS) tubes for structural and engineering applications: TS590, TS690, TS770, TS890. Tenaris, Production Brochure; 2019.
- [19] Vallourec-Mannesmann, Vallourec Seamless Steel Tubes and Pipes. Vallourec-Mannesmann, Production Brochure; 2019.
- [20] EN 10210, Hot-finished structural hollow sections of non-alloyed and fine grain. European Committee for Standardization (CEN), Brussels; 2006.
- [21] EN 1993-1-2, Eurocode 3 Design of steel structures-Part 1-2: General rules – Structural fire design. European Committee for Standardization (CEN), Brussels; 2005.
- [22] EN 1993-1-1, Eurocode 3 Design of steel structures-Part 1-1: General rules and rules for buildings. European Committee for Standardization (CEN), Brussels; 2005.
- [23] EN 1993-1-6, Eurocode 3 Design of steel structures-Part 1-6: Strength and stability of shell structures. European Committee for Standardization (CEN), Brussels; 2007.
- [24] Franssen, J.M., Schleich, J.B., Cajot, L.G.. A simple model for the fire resistance of axially-loaded members according to Eurocode 3. *Journal of Constructional Steel Research* 1995;35(1):49–69.
- [25] Talamona, D., Franssen, J.M., Schleich, J.B., Kruppa, J.. Stability of steel columns in case of fire: Numerical modeling. *Journal of Structural Engineering*, ASCE 1997;123(6):713–720.
- [26] Franssen, J.M., Talamona, D., Kruppa, J., Cajot, L.G.. Stability of steel columns in case of fire: Experimental evaluation. *Journal of Structural Engineering*, ASCE 1998;124(2):158–163.
- [27] FIDESC4. Fire design of steel members with welded or hot-rolled Class 4 cross-sections. Final report, Research program of the European Commission Research Fund for Coal and Steel; 2015.
- [28] Prachar, M., Jandera, M., Wald, F., Zhao, B.. Lateral torsional-buckling of class 4 steel plate beams at elevated temperature: Experimental and numerical comparison. *Journal of Structural Fire Engineering* 2015;6(3):223–236.
- [29] Couto, C., Real, P.V., Lopes, N., Zhao, B.. Resistance of steel cross-sections with local buckling at elevated temperatures. *Journal of Constructional Steel Research* 2015;109:101–114.
- [30] Franssen, J.M., Zhao, B., Gernay, T.. Experimental tests and numerical modelling on slender steel columns at high temperatures. *Journal of Structural Fire Engineering* 2016;7(1):30–40.
- [31] Prachar, M., Hricak, J., Jandera, M., Wald, F., Zhao, B.. Experiments of class 4 open section beams at elevated temperature. *Thin-Walled Structures* 2016;98:2–18.
- [32] Maia, É., Couto, C., Real, P.V., Lopes, N.. Critical temperatures of class 4 cross-sections. *Journal of Constructional Steel Research* 2016;121:370–382.
- [33] Couto, C., Real, P.V., Lopes, N., Zhao, B.. Numerical investigation of the lateral-torsional buckling of beams with slender cross sections for the case of fire. *Engineering Structures* 2016;106:410–421.
- [34] Couto, C., Real, P.V., Lopes, N., Zhao, B.. Local buckling in laterally restrained steel beam-columns in case of fire. *Journal of Constructional Steel Research* 2016;122:543–556.
- [35] Couto, C., Maia, É., Real, P.V., Lopes, N.. The effect of non-uniform bending on the lateral

- stability of steel beams with slender cross-section at elevated temperatures. *Engineering Structures* 2018;163:153–166.
- [36] Jandera, M., Prachař, M., Wald, F.. Lateral-torsional buckling of class 4 section uniform and web tapered beams at elevated temperature. *Thin-Walled Structures* 2020;146:106458.
- [37] Abaqus 2018 Reference Manual. Simulia, Dassault Systemes; 2018.
- [38] Kucukler, M., Xing, Z., Gardner, L.. Behaviour and design of stainless steel I-section columns in fire. *Journal of Constructional Steel Research* 2020;165:105890.
- [39] Xing, Z., Kucukler, M., Gardner, L.. Local buckling of stainless steel plates in fire. *Thin-Walled Structures* 2020;148:106570.
- [40] Kucukler, M.. Lateral instability of steel beams in fire: Behaviour, numerical modelling and design. *Journal of Constructional Steel Research* 2019;Submitted for publication.
- [41] Kucukler, M., Gardner, L., Macorini, L.. Lateral-torsional buckling assessment of steel beams through a stiffness reduction method. *Journal of Constructional Steel Research* 2015;109:87–100.
- [42] Kucukler, M., Gardner, L.. Design of web-tapered steel beams against lateral-torsional buckling through a stiffness reduction method. *Engineering Structures* 2019;190:246–261.
- [43] Fajuyitan, O.K., Sadowski, A.J., Wade, M.A., Rotter, J.M.. Nonlinear behaviour of short elastic cylindrical shells under global bending. *Thin-Walled Structures* 2018;124:574–587.
- [44] Meng, X., Gardner, L., Sadowski, A.J., Rotter, J.M.. Elasto-plastic behaviour and design of semi-compact circular hollow sections. *Thin-Walled Structures* 2020;106486.
- [45] Crisfield, M.A.. A fast incremental/iterative solution procedure that handles “snap-through”. *Computers & Structures* 1981;13(1-3):55–62.
- [46] Ramm, E.. Strategies for tracing the nonlinear response near limit points. In: *Nonlinear finite element analysis in structural mechanics*. Springer; 1981, p. 63–89.
- [47] Rubert, A., Schaumann, P.. Structural steel and plane frame assemblies under fire action. *Fire Safety Journal* 1986;10(3):173–184.
- [48] Schneider, R., Lange, J.. Constitutive equations of structural steel S460 at high temperatures. In: *Nordic Steel Construction Conference Proceedings, Malmo, Sweden*. 2009, p. 204–211.
- [49] Choi, I.R., Chung, K.S., Kim, D.H.. Thermal and mechanical properties of high-strength structural steel HSA800 at elevated temperatures. *Materials & Design* 2014;63:544–551.
- [50] Xiong, M.X., Liew, J.Y.R.. Mechanical properties of heat-treated high tensile structural steel at elevated temperatures. *Thin-Walled Structures* 2016;98:169–176.
- [51] Fang, H., Chan, T.M.. Resistance of axially loaded hot-finished S460 and S690 steel square hollow stub columns at elevated temperatures. *Structures* 2019;17:66–73.
- [52] Mirambell, E., Real, E.. On the calculation of deflections in structural stainless steel beams: An experimental and numerical investigation. *Journal of Constructional Steel Research* 2000;54(1):109–133.
- [53] Qiang, X., Bijlaard, F., Kolstein, H.. Dependence of mechanical properties of high strength steel S690 on elevated temperatures. *Construction and Building Materials* 2012;30:73–79.
- [54] Qiang, X., Bijlaard, F.S., Kolstein, H.. Elevated-temperature mechanical properties of high strength structural steel S460N: Experimental study and recommendations for fire-resistance design. *Fire Safety Journal* 2013;55:15–21.
- [55] McCann, F., Fang, C., Gardner, L., Silvestre, N.. Local buckling and ultimate strength of slender elliptical hollow sections in compression. *Engineering Structures* 2016;111:104–118.
- [56] Ma, J.L., Chan, T.M., Young, B.. Experimental investigation on stub-column behavior of cold-formed high-strength steel tubular sections. *Journal of Structural Engineering, ASCE* 2016;142(5):04015174.
- [57] Lan, X., Chen, J., Chan, T.M., Young, B.. The continuous strength method for the design of high strength steel tubular sections in compression. *Engineering Structures* 2018;162:177–187.
- [58] Toffolon, A., Taras, A.. Numerical investigation of the local buckling behaviour of high strength steel circular hollow sections. In: *Proceedings of Eurosteel 2017, Copenhagen, Denmark; vol. 1*. 2017, p. 3603–3612.
- [59] EN 1993-1-5, Eurocode 3 Design of steel structures-Part 1-5: Plated structural elements. European



- Committee for Standardization (CEN), Brussels; 2005.
- [60] Wei, S., Mau, S., Vipulanandan, C., Mantrala, S.. Performance of new sandwich tube under axial loading: Experiment. *Journal of Structural Engineering*, ASCE 1995;121(12):1806–1814.
  - [61] Pires, T.A.C., Rodrigues, J.P.C., Silva, J.J.R.. Fire resistance of concrete filled circular hollow columns with restrained thermal elongation. *Journal of Constructional Steel Research* 2012;77:82–94.
  - [62] O’Shea, M.D., Bridge, R.Q.. Local buckling of thin-walled circular steel sections with or without internal restraint. *Journal of Constructional Steel Research* 1997;41(2-3):137–157.
  - [63] Correia, A.M., Pires, T.A.C., Rodrigues, J.P.C.. Behaviour of steel columns subjected to fire. In: *Sixth International Seminar on Fire and Explosion Hazards*. 2010, p. 879–890.
  - [64] Rotter, J.M.. Cylindrical shells under axial compression. In: *Buckling of thin metal shells*. CRC Press; 2006, p. 66–111.
  - [65] Rotter, J.M.. Shell buckling design and assessment and the LBA-MNA methodology. *Stahlbau* 2011;80(11):791–803.
  - [66] Rotter, J.M.. The elastic-plastic imperfection sensitivity of axially compressed cylinders with weld depressions. In: *Proc., Eurosteel 2008 Conf.* 2008, p. 1497–1502.
  - [67] Kruppa, J.. Eurocodes–Fire parts: Proposal for a methodology to check the accuracy of assessment methods. CEN TC 250, Horizontal Group Fire, Document no: 99/130; 1999.
  - [68] Ibañez, C., Aguado, J.V., Romero, M.L., Espinos, A., Hospitaler, A.. Fire design method for concrete filled tubular columns based on equivalent concrete core cross-section. *Fire Safety Journal* 2015;78:10–23.
  - [69] Ibañez, C., Romero, M.L., Hospitaler, A.. Effects of axial and rotational restraints on concrete-filled tubular columns under fire. *Journal of Constructional Steel Research* 2016;125:114–127.
  - [70] Albero, V., Espinos, A., Romero, M.L., Hospitaler, A., Bihina, G., Renaud, C.. Proposal of a new method in EN1994-1-2 for the fire design of concrete-filled steel tubular columns. *Engineering Structures* 2016;128:237–255.
  - [71] Lopes, N., Manuel, M., Sousa, A.R., Real, P.V.. Parametric study on austenitic stainless steel beam-columns with hollow sections under fire. *Journal of Constructional Steel Research* 2019;152:274–283.

## Figures captions

Figure 1 : Details of the finite element models of CHS stub columns and columns developed in this study

Figure 2 : Stress-strain relationship and material property reduction factors for carbon steel at elevated temperatures adopted in this study as given in [21]

Figure 3 : Comparison of the Young's modulus reduction factors  $k_{E,\theta}$  and yield strength reduction factors  $k_{y,\theta}$  for grade S690, S460, S355, S275 and S235 steels adopted in this study

Figure 4 : Elevated temperature stress-strain response of S690 and S460 grade steels at different elevated temperature levels obtained by [53, 54] and material model adopted in the finite element models

Figure 5 : Comparison of the axial deformation versus time paths obtained from the fire experiments carried out on high-strength steel CHS columns by Tondini et al. [15] and those determined through the finite element models created in this study

Figure 6 : Comparison of the failure mode of C1 CHS high-strength steel column specimen observed in the experiment of Tondini et al. [15] and that determined through the finite element model of the specimen created in this study

Figure 7 : Comparison of the axial stress versus axial strain paths obtained from the experiments carried out on high-strength steel CHS stub columns by Wei et al. [60] at room temperature against those determined through the finite element models created in this study

Figure 8 : Comparison of the axial deformation versus time paths obtained from the fire experiments carried out on normal-strength steel CHS columns by Pires et al. [61] and those determined through the finite element models created in this study

Figure 9 : Comparison of the axial stress normalised by the yield strength versus axial strain paths obtained from the experiments carried out on normal-strength steel CHS stub columns by O'Shea and Bridge [62] at room temperature against those determined through the finite element models created in this study

Figure 10 : Accuracy of EN 1993-1-2 [21] for the ultimate strength predictions of CHS stub columns in fire

Figure 11 : Accuracy of EN 1993-1-2 [21] for the ultimate strength predictions of CHS columns in fire

Figure 12 : Accuracy of EN 1993-1-2 [21] for the ultimate strength predictions of CHS

columns with Class 1, 2 and 3 sections in fire

Figure 13 : Accuracy of the proposed design method for cross-section axial compression resistances of CHS members at elevated temperatures

Figure 14 : Accuracy of the proposed design method against EN 1993-1-2 [21] for the ultimate cross-section axial compression resistance predictions of CHS members in fire

Figure 15 : Accuracy of the proposed design method for the flexural buckling resistance predictions of CHS steel columns at elevated temperatures

Figure 16 : Accuracy of the proposed design method for the flexural buckling resistance predictions of CHS steel columns with Class 1, 2 and 3 sections at elevated temperatures

Figure 17 : Accuracy of the proposed design method against EN 1993-1-2 [21] for flexural buckling strength predictions of CHS columns in fire

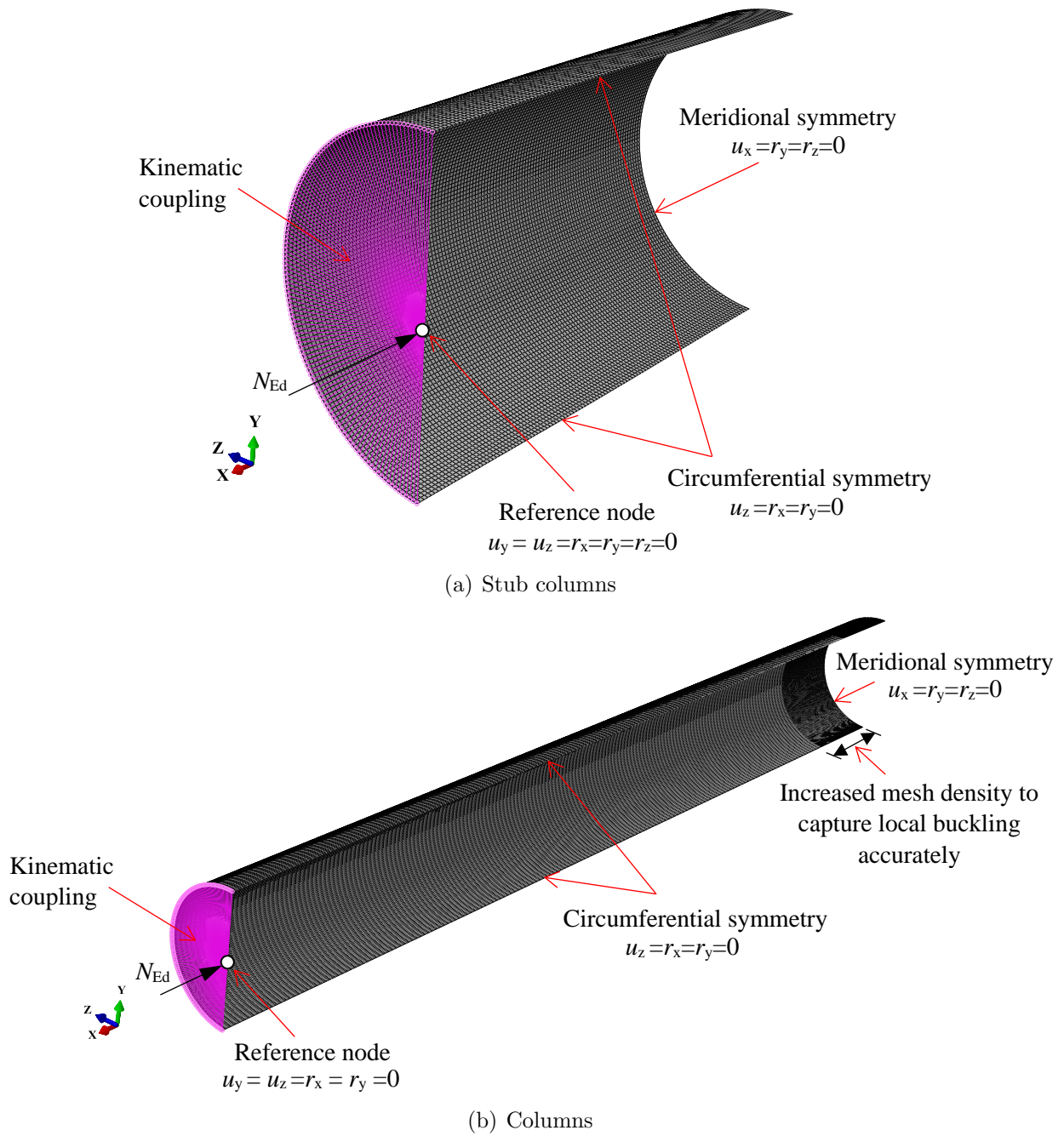


Figure 1: Details of the finite element models of CHS stub columns and columns developed in this study

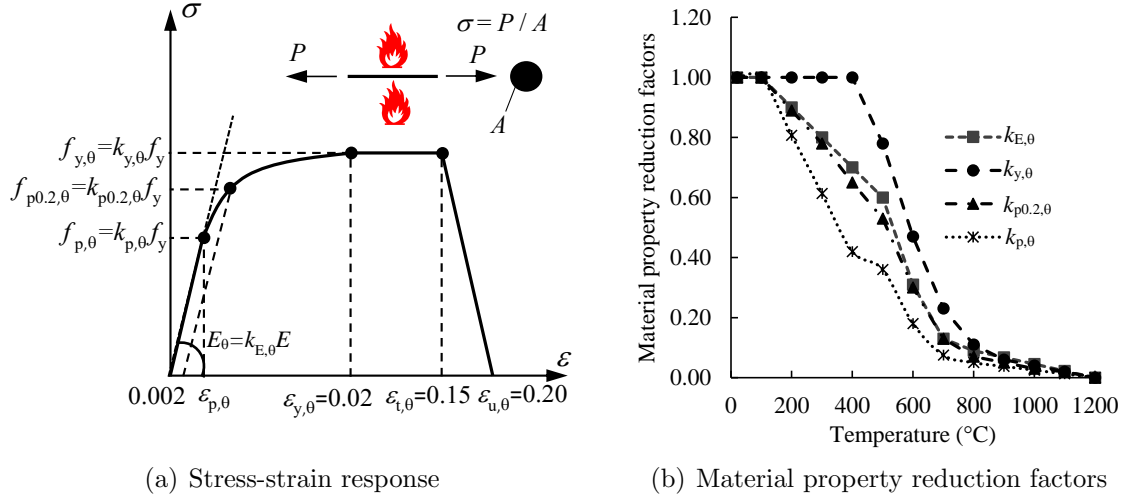


Figure 2: Stress-strain relationship and material property reduction factors for carbon steel at elevated temperatures adopted in this study as given in [21]

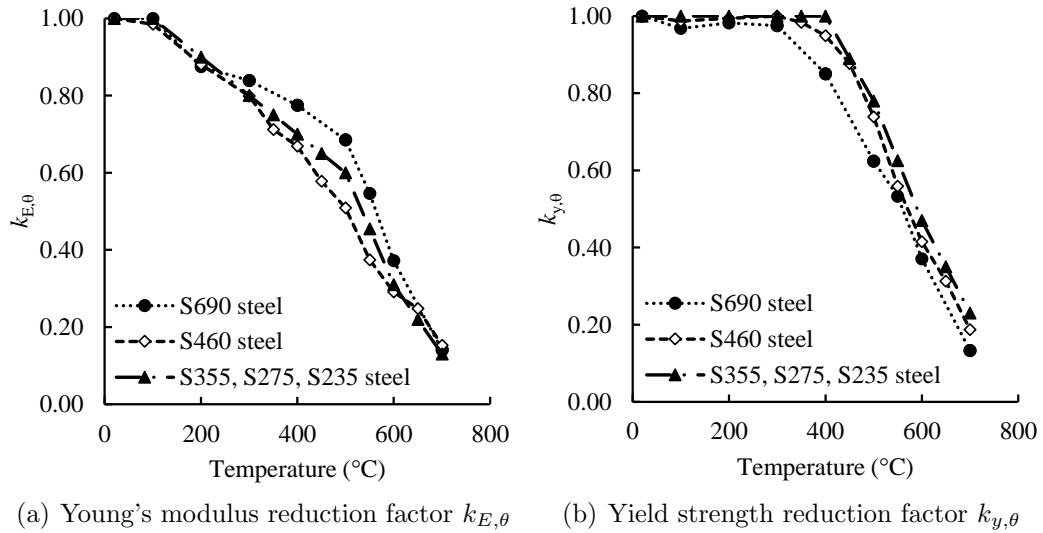
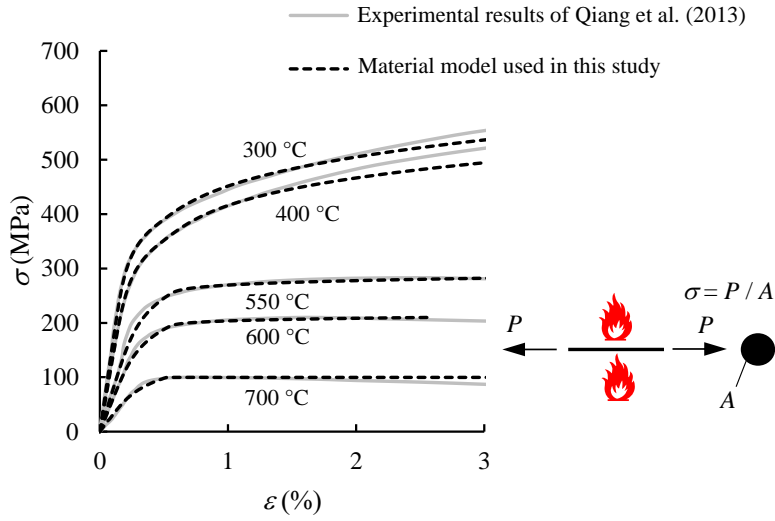
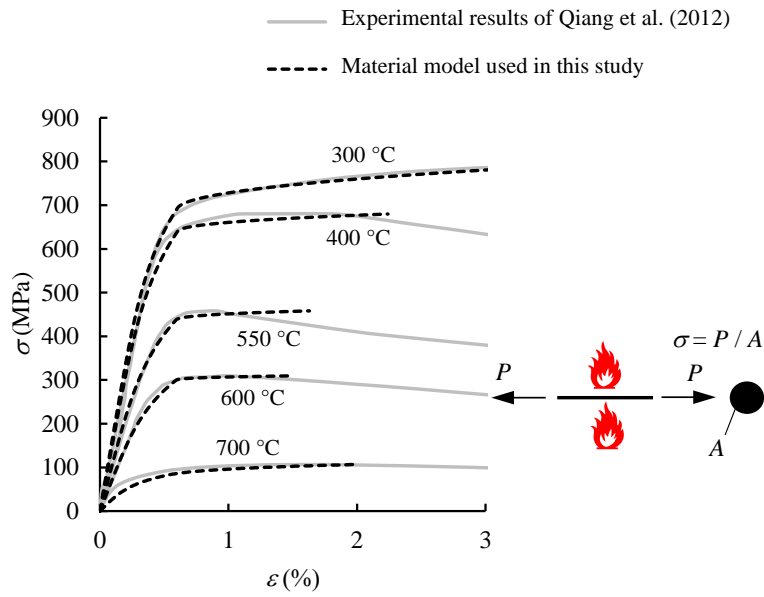


Figure 3: Comparison of the Young's modulus reduction factors  $k_{E,\theta}$  and yield strength reduction factors  $k_{y,\theta}$  for grade S690, S460, S355, S275 and S235 steels adopted in this study

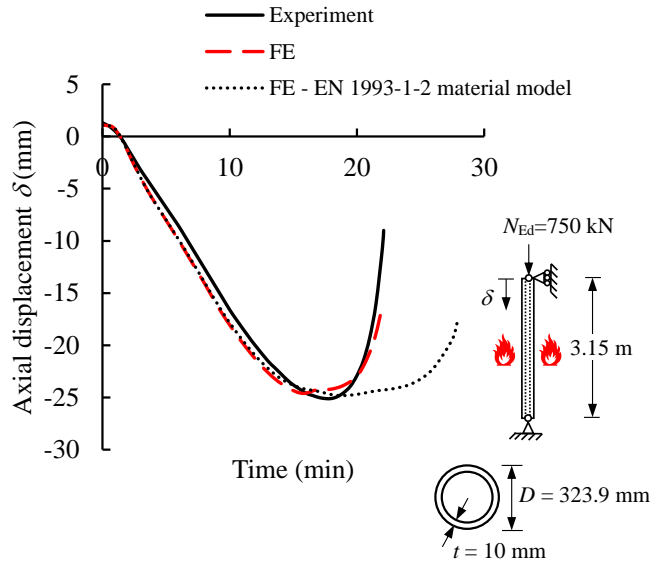


(a) S460

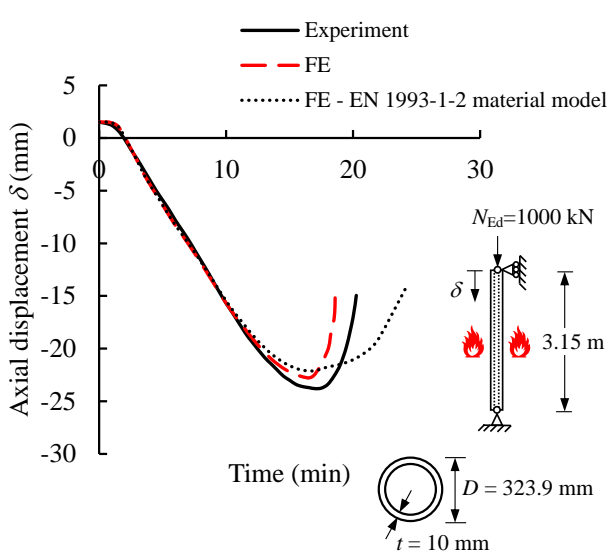


(b) S690

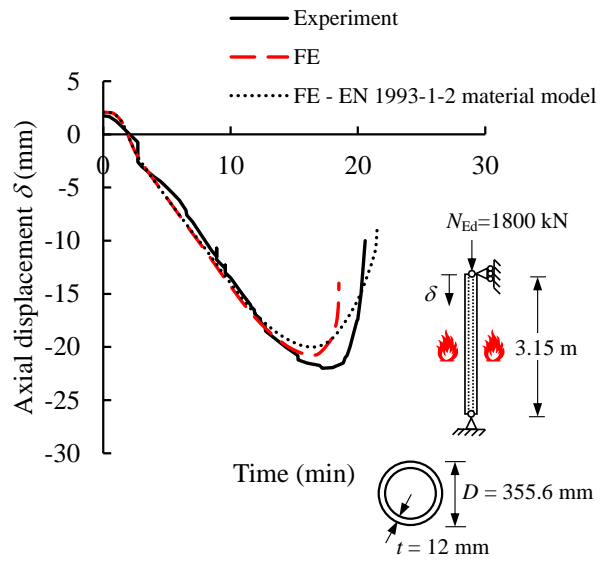
Figure 4: Elevated temperature stress-strain response of S690 and S460 grade steels at different elevated temperature levels obtained by [53, 54] and material model adopted in the finite element models



(a) C1 specimen



(b) C2 specimen



(c) C3 specimen

Figure 5: Comparison of the axial deformation versus time paths obtained from the fire experiments carried out on high-strength steel CHS columns by Tondini et al. [15] and those determined through the finite element models created in this study



(a) Experiment



(b) FE

Figure 6: Comparison of the failure mode of C1 CHS high-strength steel column specimen observed in the experiment of Tondini et al. [15] and that determined through the finite element model of the specimen created in this study



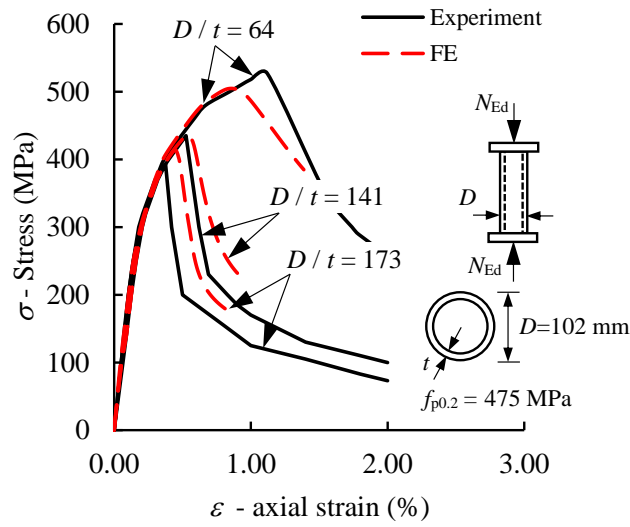
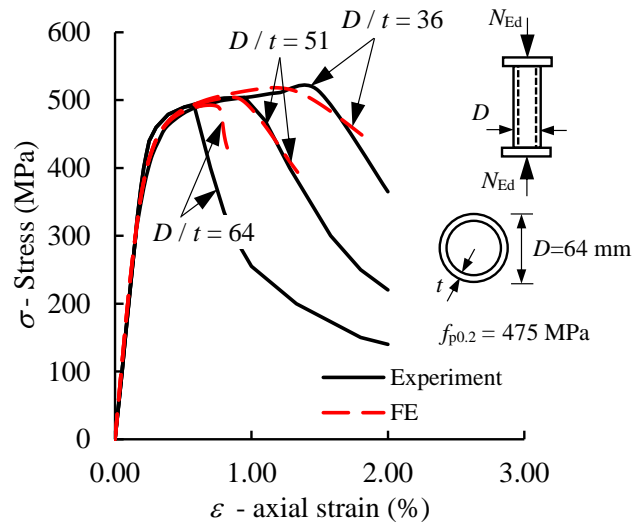


Figure 7: Comparison of the axial stress versus axial strain paths obtained from the experiments carried out on high-strength steel CHS stub columns by Wei et al. [60] at room temperature against those determined through the finite element models created in this study

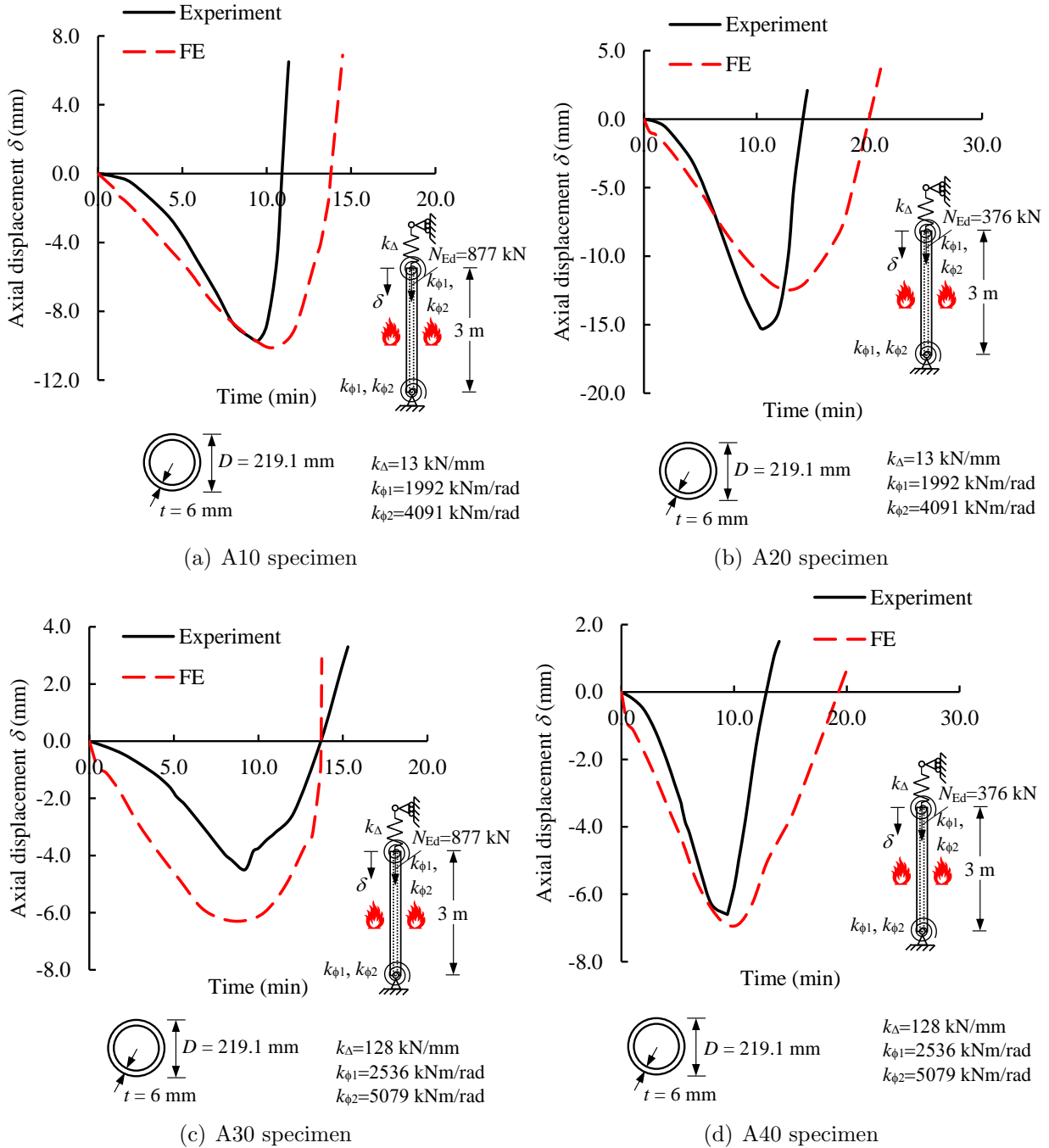


Figure 8: Comparison of the axial deformation versus time paths obtained from the fire experiments carried out on normal-strength steel CHS columns by Pires et al. [61] and those determined through the finite element models created in this study

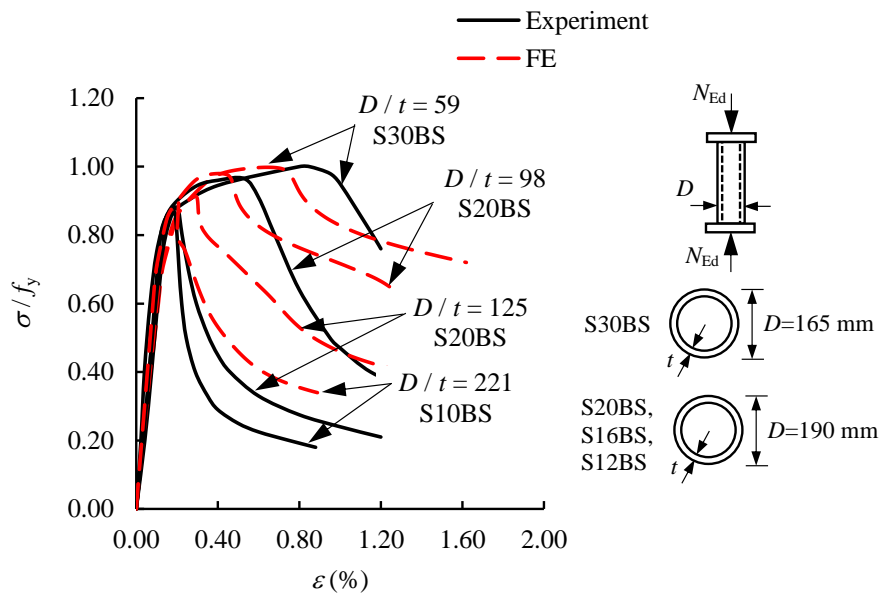


Figure 9: Comparison of the axial stress normalised by the yield strength versus axial strain paths obtained from the experiments carried out on normal-strength steel CHS stub columns by O’Shea and Bridge [62] at room temperature against those determined through the finite element models created in this study

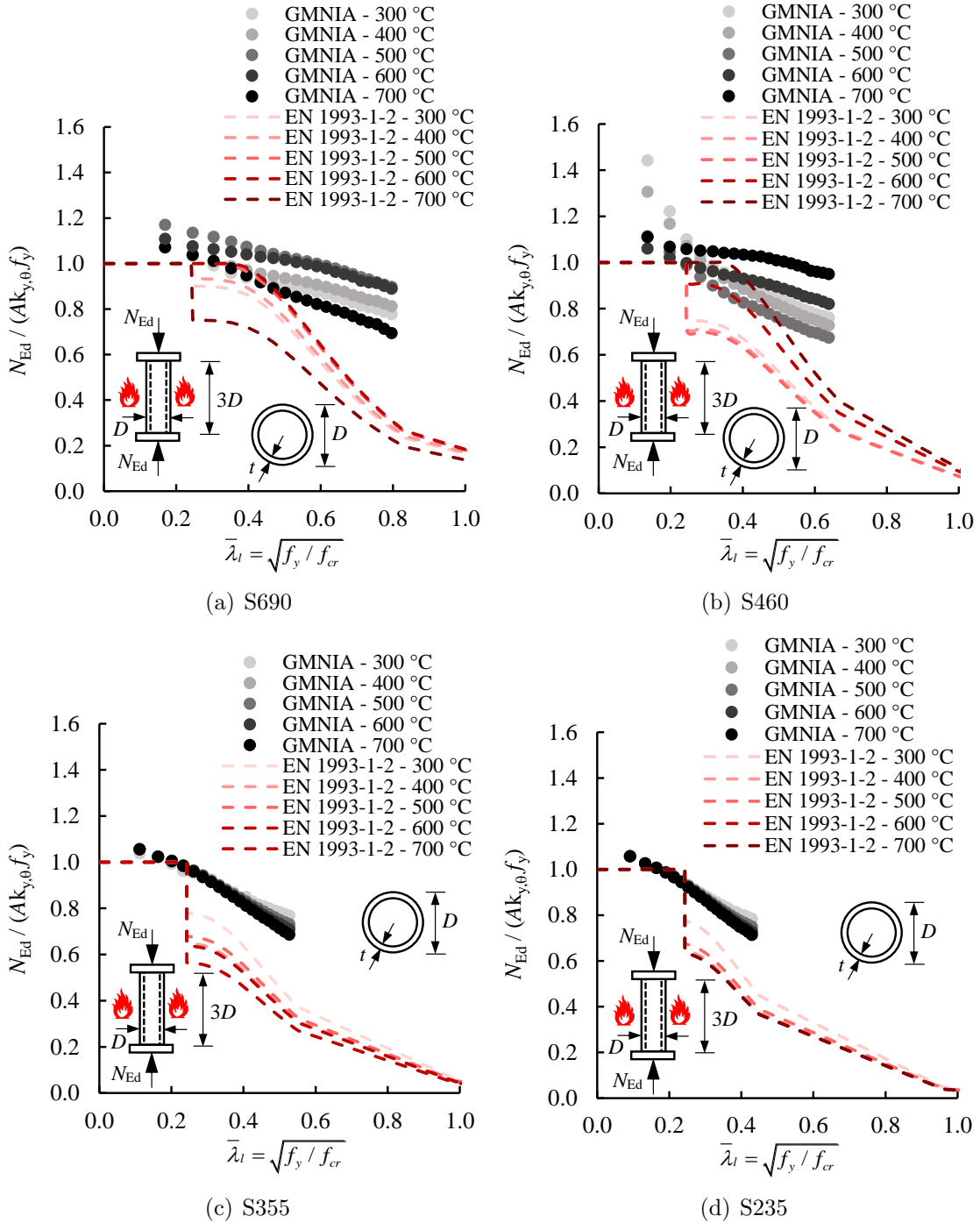


Figure 10: Accuracy of EN 1993-1-2 [21] for the ultimate strength predictions of CHS stub columns in fire

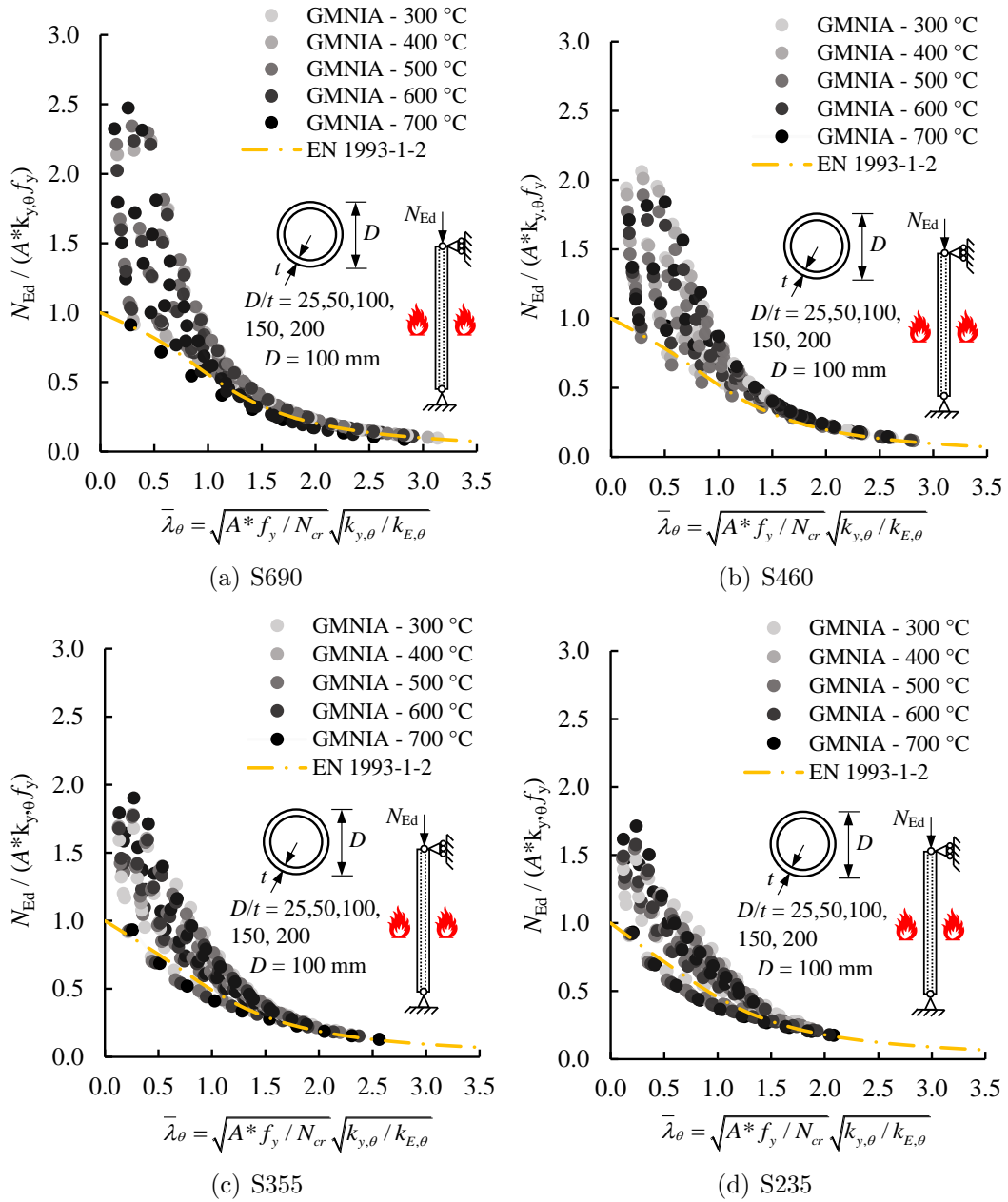
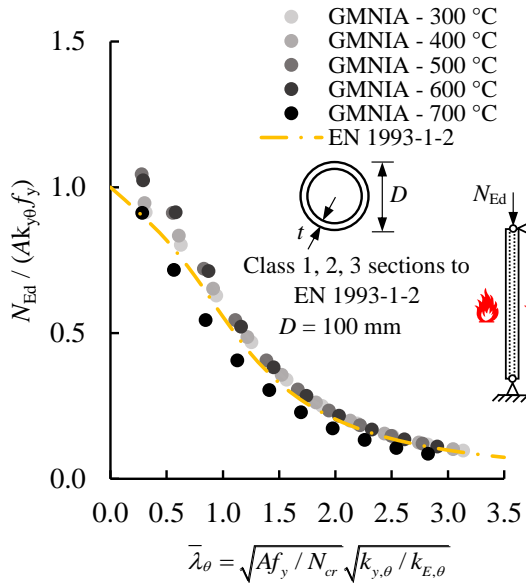
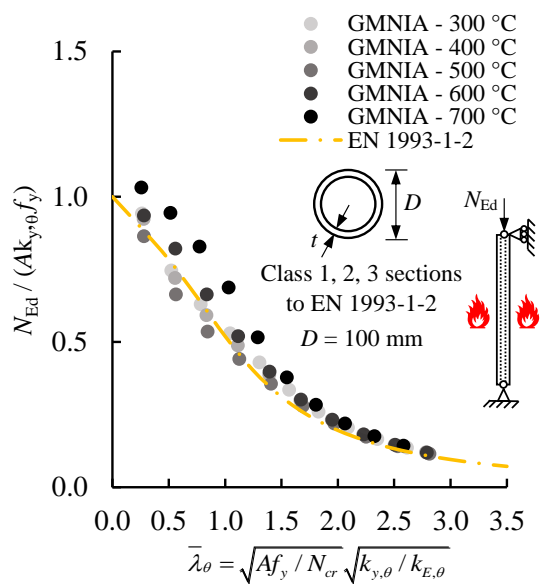


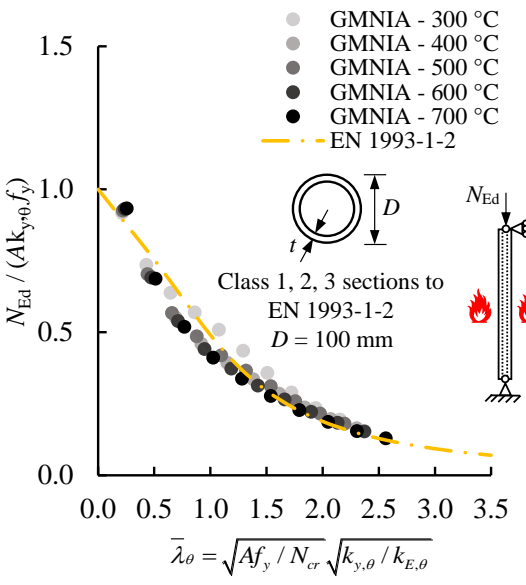
Figure 11: Accuracy of EN 1993-1-2 [21] for the ultimate strength predictions of CHS columns in fire



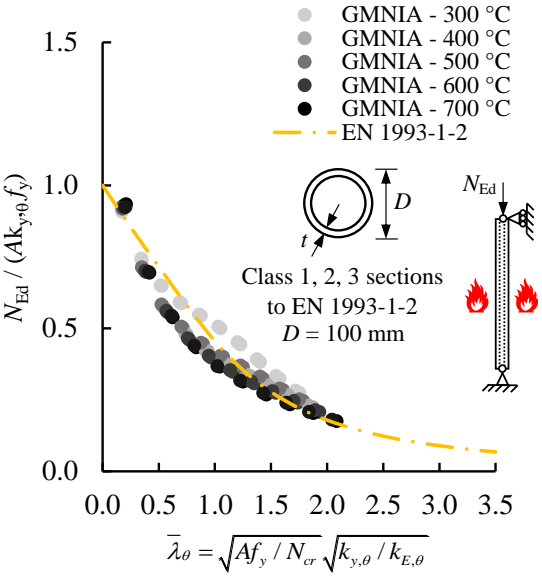
(a) S690



(b) S460



(c) S355



(d) S235

Figure 12: Accuracy of EN 1993-1-2 [21] for the ultimate strength predictions of CHS columns with Class 1, 2 and 3 sections in fire

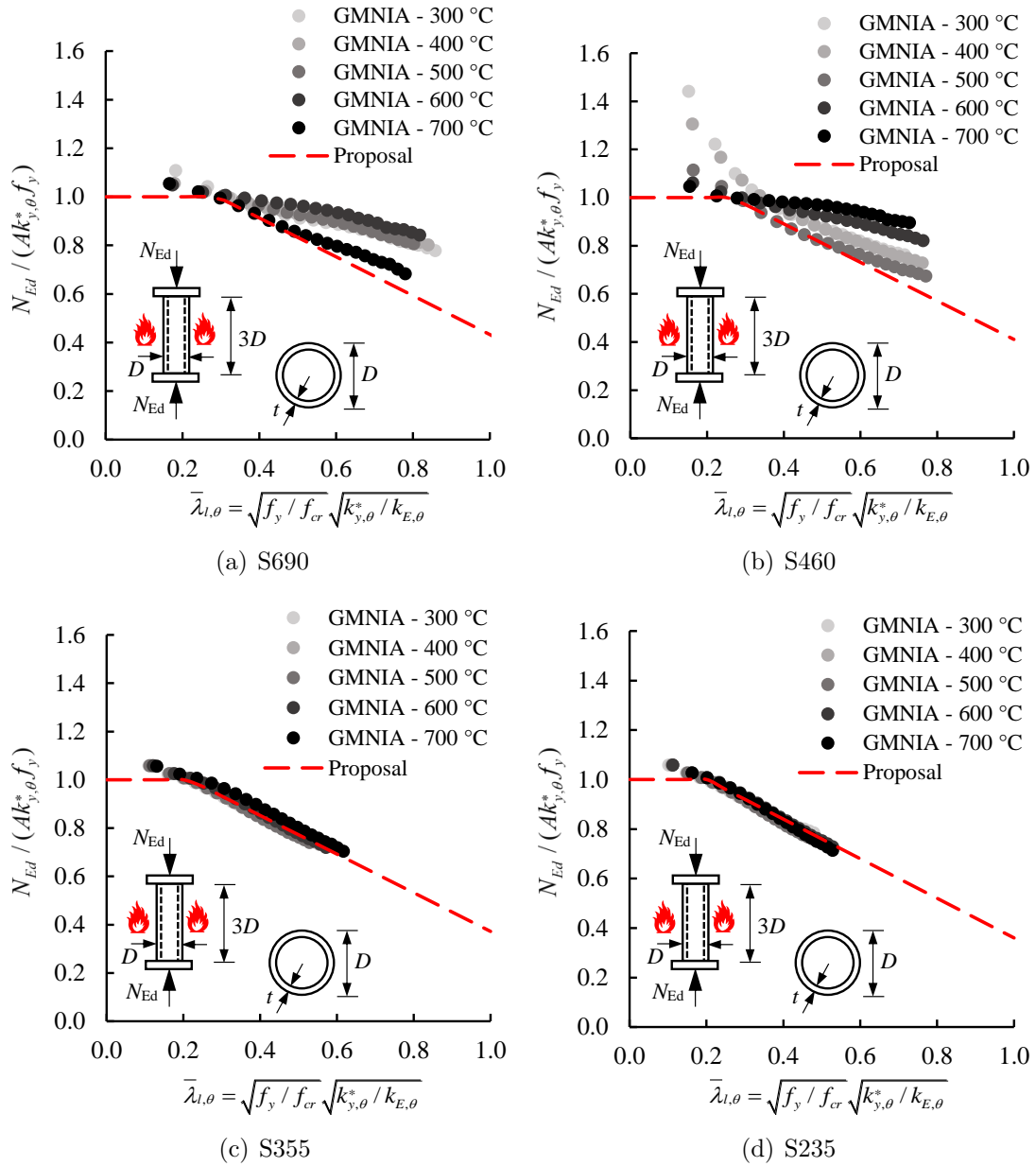


Figure 13: Accuracy of the proposed design method for cross-section axial compression resistances of CHS members at elevated temperatures

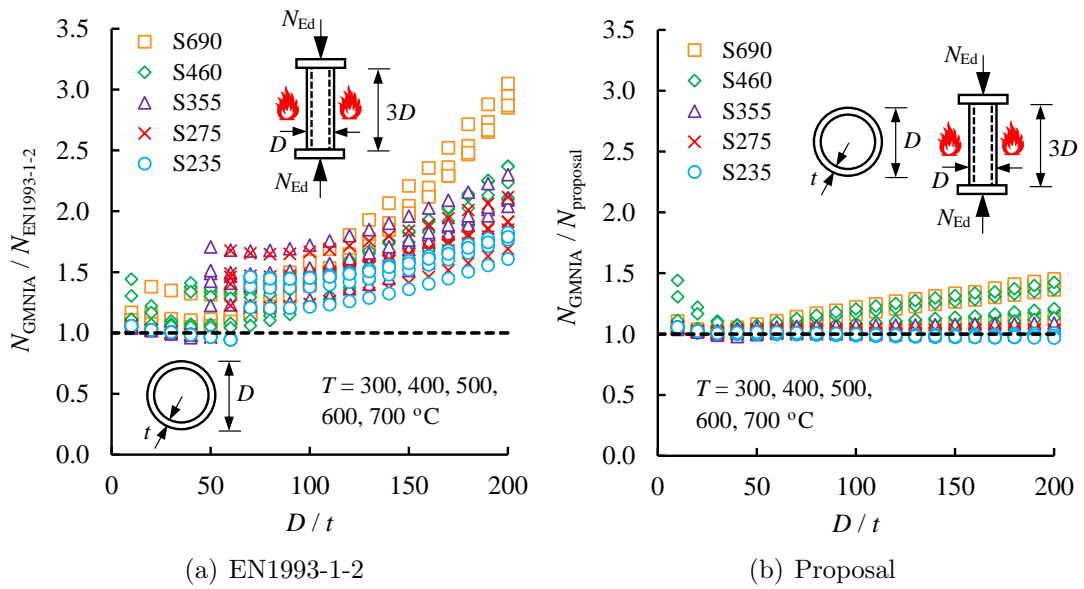


Figure 14: Accuracy of the proposed design method against EN 1993-1-2 [21] for the ultimate cross-section axial compression resistance predictions of CHS members in fire



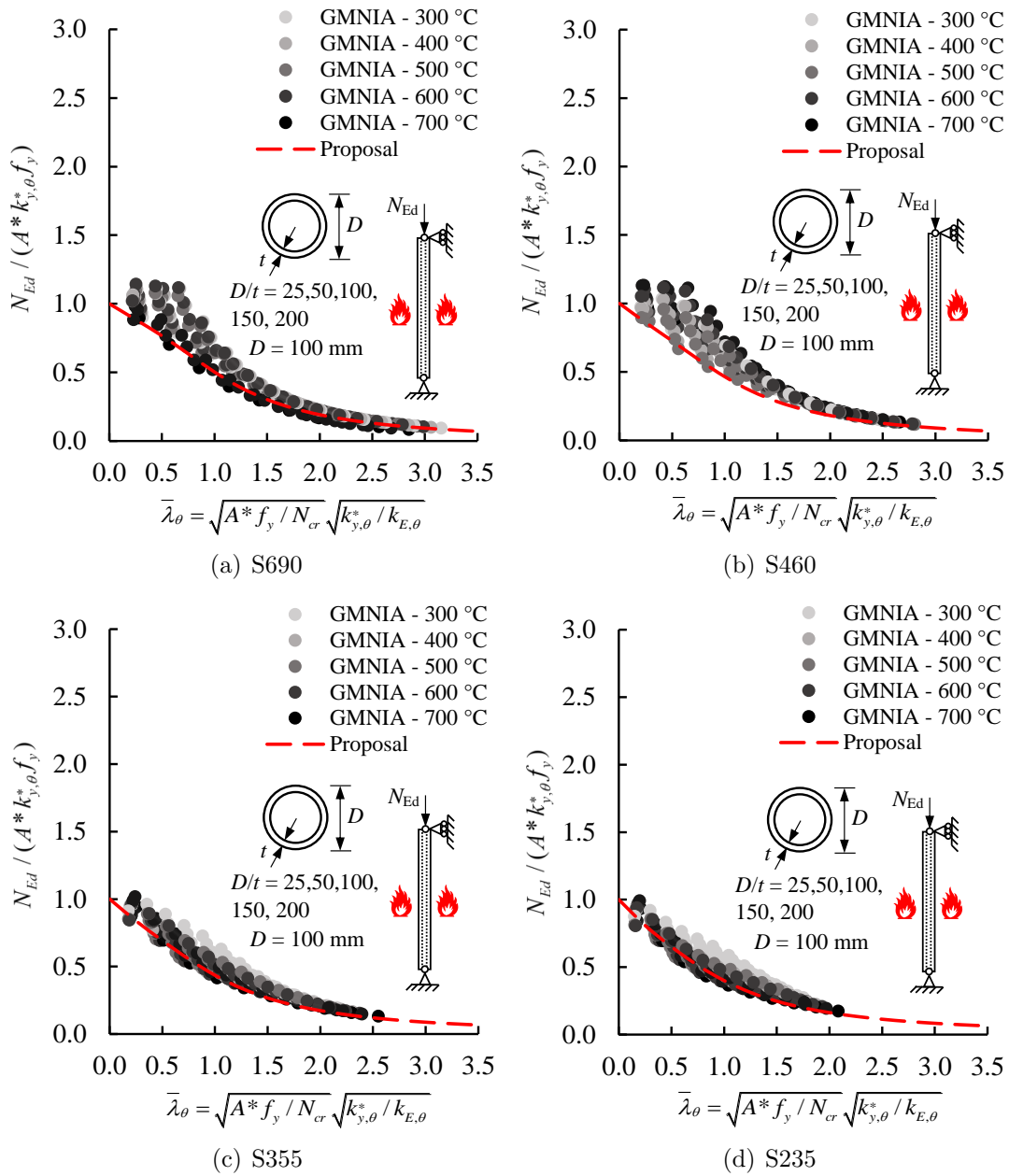


Figure 15: Accuracy of the proposed design method for the flexural buckling resistance predictions of CHS steel columns at elevated temperatures

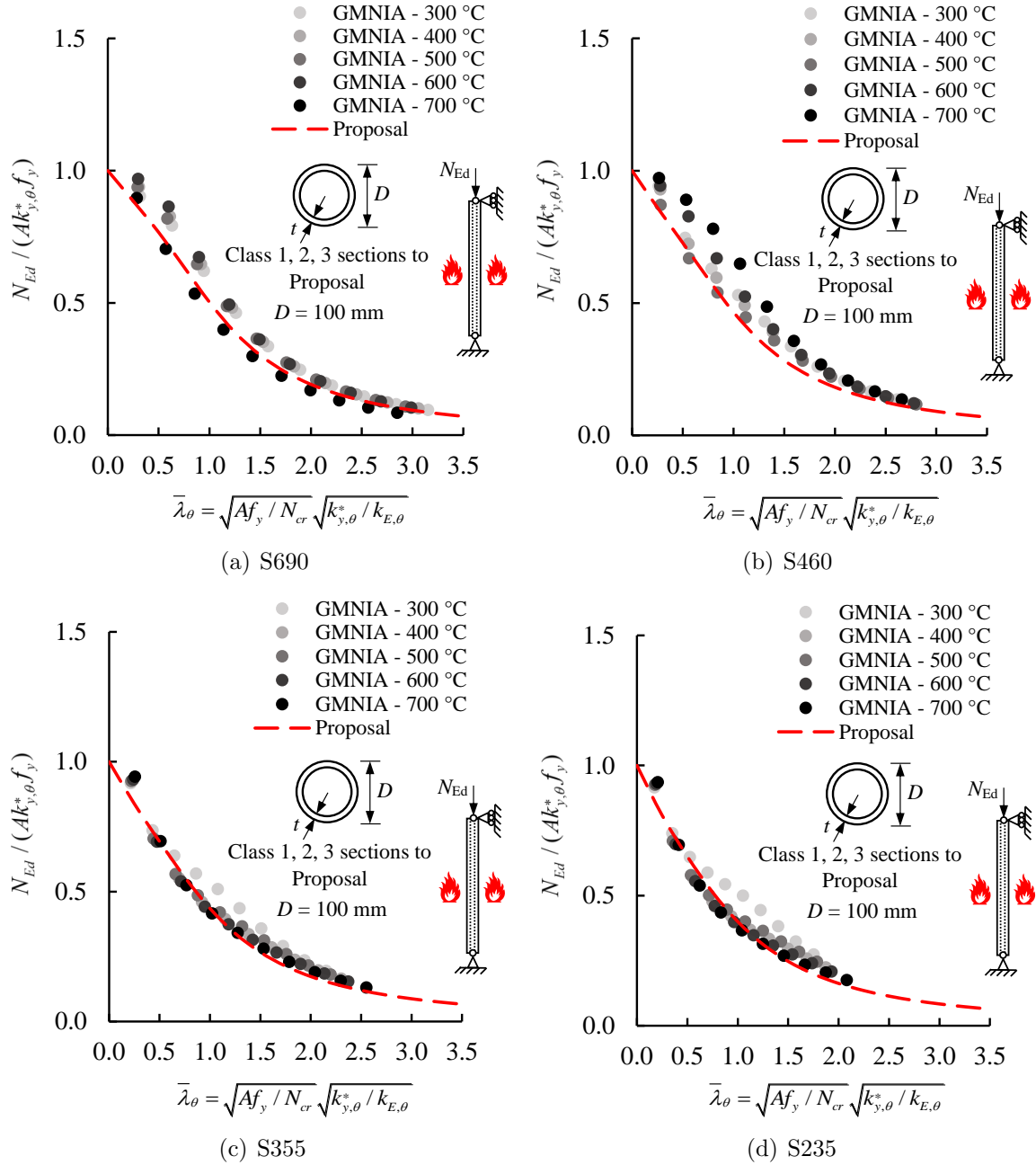
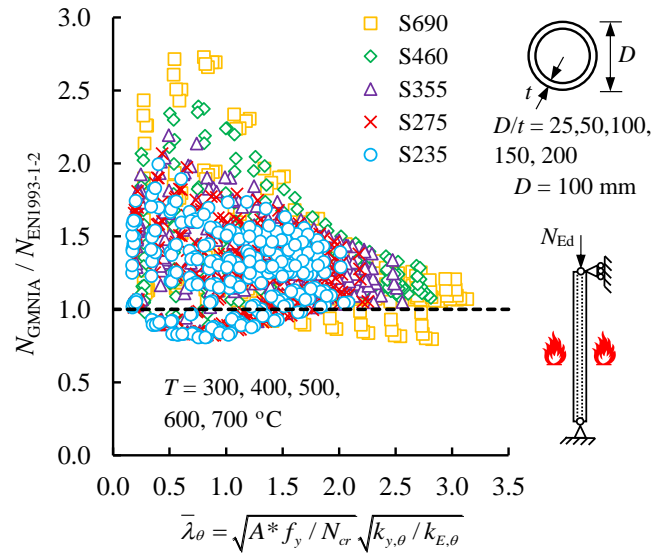
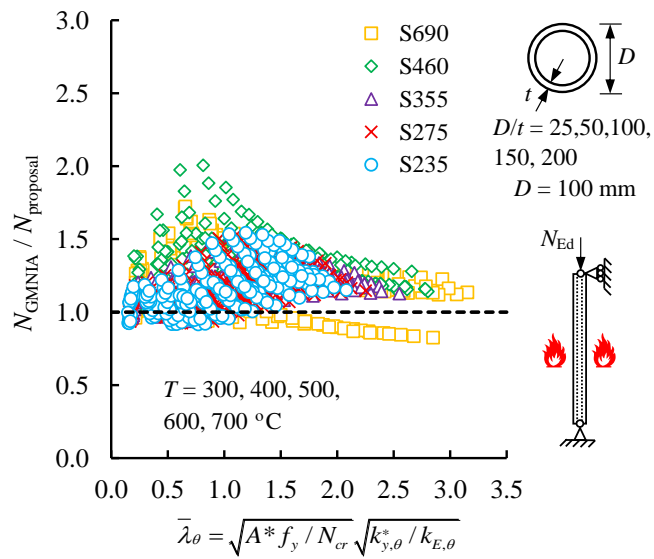


Figure 16: Accuracy of the proposed design method for the flexural buckling resistance predictions of CHS steel columns with Class 1, 2 and 3 sections at elevated temperatures



(a) EN1993-1-2



(b) Proposal

Figure 17: Accuracy of the proposed design method against EN 1993-1-2 [21] for flexural buckling strength predictions of CHS columns in fire

## Tables captions

Table 1 : Material reduction factors derived by Qiang et al. [53] and Ramberg-Osgood exponents used in this study for grade S690 steel ( $E = 204690$  MPa,  $f_y=789$  MPa,  $\sigma_u=821$  MPa and  $\epsilon_u=0.051$ )

Table 2 : Material reduction factors derived by Qiang et al. [54] and Ramberg-Osgood exponents used in this study for grade S460 steel ( $E = 202812$  MPa,  $f_y=504$  MPa,  $\sigma_u=640$  MPa and  $\epsilon_u=0.115$ )

Table 3 : Summary of numerical parametric studies carried out in this paper

Table 4 : Accuracy of the proposed design method against EN 1993-1-2 [21] for the ultimate cross-section axial compression resistance predictions of CHS members in fire

Table 5 : Accuracy of the proposed design method against EN 1993-1-2 [21] for flexural buckling strength predictions of CHS columns in fire

Table 6 : Assessment of the reliability of the design proposal made in this study and EN 1993-1-2 [21] on the basis of the three reliability criteria set out by Kruppa [67]. Note that the numbers denoted by \* violates the corresponding criterion

Table 1: Material reduction factors derived by Qiang et al. [53] and Ramberg-Osgood exponents used in this study for grade S690 steel ( $E = 204690$  MPa,  $f_y=789$  MPa,  $\sigma_u=821$  MPa and  $\epsilon_u=0.051$ )

Temperature ( $^{\circ}\text{C}$ )	$k_{E,\theta}$	$k_{p0.2,\theta}$	$k_{y,\theta}$	$k_{u,\theta}$	$k_{\epsilon_u,\theta}$	$n_\theta$	$m_\theta$
200	0.875	0.884	0.982	0.991	0.957	6.20	1.93
300	0.839	0.879	0.975	0.961	0.696	5.80	2.10
400	0.775	0.794	0.850	0.828	0.280	5.40	2.27
500	0.685	0.628	0.624	0.628	0.161	5.00	2.43
550	0.546	0.554	0.533	0.558	0.178	4.80	2.52
600	0.372	0.380	0.371	0.377	0.196	4.60	2.60
700	0.141	0.100	0.133	0.130	0.333	4.20	2.77

Table 2: Material reduction factors derived by Qiang et al. [54] and Ramberg-Osgood exponents used in this study for grade S460 steel ( $E = 202812$  MPa,  $f_y=504$  MPa,  $\sigma_u=640$  MPa and  $\epsilon_u=0.115$ )

Temperature ( $^{\circ}\text{C}$ )	$k_{E,\theta}$	$k_{p0.2,\theta}$	$k_{y,\theta}$	$k_{u,\theta}$	$k_{\epsilon_u,\theta}$	$n_\theta$	$m_\theta$
200	0.881	0.812	0.994	0.969	0.758	10.00	2.70
300	0.799	0.750	1.000	1.000	0.804	9.00	3.00
400	0.669	0.681	0.949	0.880	0.517	8.00	3.30
500	0.509	0.520	0.739	0.601	0.296	7.00	3.60
550	0.374	0.496	0.559	0.443	0.217	6.50	3.75
600	0.291	0.379	0.415	0.328	0.139	6.00	3.90
700	0.153	0.196	0.187	0.157	0.066	5.00	4.20

Table 3: Summary of numerical parametric studies carried out in this paper

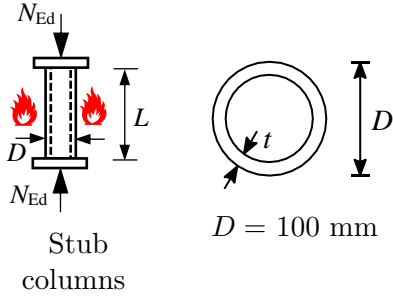
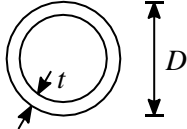
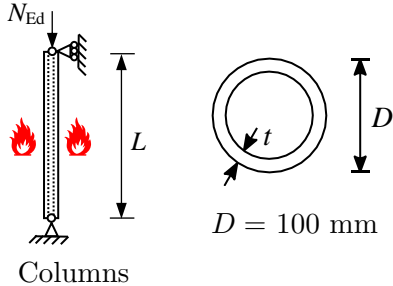
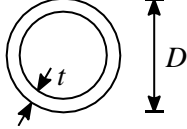
	Cross-section	$L/D$	$D/t$	Steel grade	Temperature
 <p>Stub columns</p>	 <p><math>D = 100</math> mm</p>	3	10 to 200 with $\Delta D/t = 10$	S690	300 °C
				S460	400 °C
				S355	500 °C
				S275	600 °C
				S235	700 °C
 <p>Columns</p>	 <p><math>D = 100</math> mm</p>	5 to 50 with $\Delta L/D = 5$	25, 50, 100, 150, 200	S690	300 °C
				S460	400 °C
				S355	500 °C
				S275	600 °C
				S235	700 °C

Table 4: Accuracy of the proposed design method against EN 1993-1-2 [21] for the ultimate cross-section axial compression resistance predictions of CHS members in fire

	Steel grade	N	$\epsilon_{av}$	$\epsilon_{COV}$	$\epsilon_{max}$	$\epsilon_{min}$
EN 1993-1-2 [21]	S690	100	1.69	0.346	3.05	1.05
	S460	100	1.51	0.243	2.37	0.99
	S355	100	1.50	0.214	2.11	0.96
	S275	100	1.41	0.204	1.92	0.96
	S235	100	1.35	0.197	1.83	0.94
Proposal	S690	100	1.17	0.112	1.45	1.00
	S460	100	1.14	0.095	1.44	0.99
	S355	100	1.03	0.019	1.08	0.98
	S275	100	1.01	0.018	1.06	0.99
	S235	100	1.00	0.019	1.06	0.97

Table 5: Accuracy of the proposed design method against EN 1993-1-2 [21] for flexural buckling strength predictions of CHS columns in fire

	Steel grade	N	$\epsilon_{av}$	$\epsilon_{COV}$	$\epsilon_{max}$	$\epsilon_{min}$
EN 1993-1-2 [21]	S690	250	1.34	0.311	2.73	0.80
	S460	250	1.37	0.225	2.39	0.88
	S355	250	1.35	0.205	2.19	0.84
	S275	250	1.27	0.221	2.07	0.82
	S235	250	1.25	0.218	1.99	0.81
Proposal	S690	250	1.23	0.143	1.72	0.83
	S460	250	1.31	0.129	2.01	0.96
	S355	250	1.18	0.103	1.53	0.94
	S275	250	1.16	0.118	1.53	0.92
	S235	250	1.15	0.129	1.54	0.92
Proposal – $\alpha = 0.65\sqrt{235/f_y}$	S690	250	1.15	0.137	1.59	0.79
	S460	250	1.20	0.120	1.81	0.89
	S355	250	1.08	0.097	1.35	0.84
	S275	250	1.05	0.111	1.35	0.82
	S235	250	1.04	0.121	1.36	0.81

Table 6: Assessment of the reliability of the design proposal made in this study and EN 1993-1-2 [21] on the basis of the three reliability criteria set out by Kruppa [67]. Note that the numbers denoted by \* violates the corresponding criterion

	Steel Grade	Criterion 1	Criterion 2	Criterion 3
EN 1993-1-2 [21]	S690	3.61*	9.24	-19.86
	S460	0.00	3.24	-24.25
	S355	2.82*	8.06	-23.03
	S275	8.03*	20.08*	-17.47
	S235	9.28*	22.36*	-15.77
Proposal	S690	3.21*	12.45	-17.16
	S460	0.00	0.81	-22.34
	S355	0.00	8.87	-14.46
	S275	0.00	12.85	-12.99
	S235	0.00	16.03	-11.89
Proposal – $\alpha = 0.65\sqrt{235/f_y}$	S690	8.43*	16.47	-11.17
	S460	0.00	4.86	-15.74
	S355	2.82*	24.60*	-6.11
	S275	5.62*	32.93*	-3.79
	S235	8.44*	40.93*	-2.17